Preprint of paper published as Journal of Physics. D, Applied Physics. 51 (2018) 483002.

Screening and engineering of colour centres in diamond

Tobias Lühmann[1], Nicole Raatz[1], Roger John[1], Margarita Lesik[2], Jasper Rödiger[3], Marc Portail[4], Dominik Wildanger[5], Felix Kleissler[5], Kai Nordlund[6], Alexander Zaitsev[7], Jean-François Roch[2], Stefan W. Hell[5], Alexandre Tallaire[8,9], Jan Meijer[1] and Sébastien Pezzagna[1]

[1]Nuclear Solid-State Physics, Felix-Bloch Institute for Solid-State Physics, University Leipzig, Linnéstraße 5, 04103 Leipzig, Germany
[2]Laboratoire Aimé Cotton, CNRS, Université Paris-Sud and Ecole Normale Supérieure de Cachan, 91405 Orsay, France
[3]Fraunhofer Heinrich Hertz Institute, Einsteinufer 37, 10587 Berlin, Germany
[4]Centre de Recherche sur l´Hétéro-Epitaxie et ses Applications, Rue Bernard Grégory, 06560 Valbonne, France
[5]Department of NanoBiophotonics, Max Planck Institute for Biophysical Chemistry, Am Faßberg 11, 37077 Göttingen, Germany
[6]Department of Physics and Helsinki Institute of Physics, University of Helsinki, Finland
[7]The College of Staten Island, City University of New York, 2800 Victory Blvd, Staten Island, NY 10314, USA
[8]Laboratoire des Sciences des Procédés et Matériaux, Université Paris 13, Sorbonne Paris Cité, CNRS, 93430 Villetaneuse, France
[9]IRCP Paris, 11 rue Pierre et Marie Curie, 75005 Paris, France

Abstract

We present a high throughput and systematic method for screening of colour centres in diamond. We aim at the search and reproducible creation of new optical centres, down to the single level, potentially of interest for the wide range of diamond-based quantum applications. The screening method presented here should moreover help identifying some already indexed defects among hundreds in diamond [1] but also some promising defects of still unknown nature, such as the recently discovered ST1 centre [2,3]. We use ion implantation in a systematic manner to implant several chemical elements. Ion implantation has the advantage to address single atoms inside the bulk with defined depth and high lateral resolution, but the disadvantage of defect production such as vacancies. The sample is annealed in vacuum at different temperatures (between 600°C and 1600°C with 200°C steps) and fully characterised at each step in order to follow the evolution of the defects: formation, dissociation, diffusion, re-formation and charge state, at the ensemble level and, if possible, at the single centre level. We review the unavoidable ion implantation defects (with the example of the GR1 and 3H centres), discuss ion channeling and thermal annealing and estimate the diffusion of vacancies, nitrogen and hydrogen. We use different characterisation methods best suited for our study (from widefield fluorescence down to sub-diffraction optical imaging of single centres) and discuss reproducibility issues due to diamond and defect inhomogeneities. Nitrogen is also implanted as a reference, taking advantage of the large knowledge on NV centres as a versatile sensor in order to retrieve or deduce the conditions and local environment in which the different implanted chemical elements are embedded. We show here the preliminary promising results of a long-term study and focus on the elements O, Mg, Ca, F and P, from which fluorescent centres were found.

Contents

Introduction

The emergence of quantum information processing and the search for suitable systems and hosts have shed light on defect-related optical centres in solid-state materials. Colour centres behave like single artificial atoms and, compared to alternative approaches like quantum dots, they can be fabricated in a well-defined way with similar properties. To achieve long coherence times even at room temperature, it is important that the host material has a wide bandgap (to avoid free charge carriers) and a high Debye temperature (to reduce the interaction with phonons). Diamond and more particularly the nitrogen-vacancy (NV) centre have been widely studied and demonstrated unique optical and spin properties [4,5] of great interest for a wide range of applications such as quantum computing [6,7], quantum communication [8,9] and quantum sensing of magnetic field [10-12] electric field [13] or temperature [14-16]. More recently, the possibility to reversibly tune the charge state of a single NV centre from NV^- through NV^0 to NV^+ was demonstrated [17,18], as well as the electrical readout of magnetic resonance using photocurrent measurement (PDMR) [19]. However, despite its outstanding properties, the NV centre has a large electron phonon coupling which leads to only 4% of the light emitted in the zero-phonon line (ZPL). Spectral diffusion is also a serious issue. On the other hand, the silicon-vacancy centre (SiV) possesses many advantages, such as the possibility to produce indistinguishable photons [20] due to an emission mostly found within the zero-phonon line at 737 nm. A direct coherent control of the SiV spin state requires 4K temperature to avoid phonon scattering [21,22]. However, with nano-photonic structures, it is possible to switch single photons and allow the achievement of entangled SiV centres by indistinguishable Raman photons emitted into a waveguide [23]. Recently, the attention has also been focused on other X-vacancy defects involving group IV elements. The GeV and SnV centres were both artificially created and observed down to the single centre level. The GeV centre was successfully produced both by ion implantation [24,25] and by high-pressure growth [26]. It has a sharp and strong photoluminescence band at RT with a ZPL at 602 nm

and a lifetime of about 1.4 ns with photon count rates measured up to 200 kCts/s. The GeV has a split-vacancy crystal structure similar to the one of the SiV centre. The SnV centre shows a ZPL at 620 nm at room temperature [27]. At low temperature, this line splits up into two peaks with a FWHM of 0.2 nm only [28]. The PbV centre is also expected but the large number of vacancies produced by a single Pb atom due to its large mass, may depress the production of this centre.

A promising defect centre but which has still not been reliably reproduced, so-called ST1, shows optically detected magnetic resonance (ODMR) at room temperature, which is a rare property among optical centres in diamond [2,3] only shared with the NV centre to date. The electronic level configuration consists of a singlet ground state and a triplet in the excited state. This is of advantage with respect to the NV centre, due to the fact that the singlet spin-free ground state should prevent the spin state from decoupling with the environmental spin bath. The ST1 centre does not show hyperfine coupling indicating a nuclear-spin-free constituent. One of the candidates for this defect is ^{16}O (oxygen was involved in the etching [2] and in the implantation processes [3] which led to the discovery of the ST1 centre), however there is no evidence about it. As well, ^{24}Mg or ^{40}Ca might also be involved. Interestingly, the L1 defect centre (with very sharp and bright polarised emission with ZPL at 580 nm) was produced together with the ST1 centre by ion implantation [3]. The nature of these two centres is still unknown however they may involve the same impurity atom in different configurations. Native centres emitting in the near-infrared were also reported from commercially available diamond samples treated thermally [29] without knowing what they are made of. Note that fluorescent centres related to Europium [30] and Helium [31,32] were recently reported.

Therefore, a large number of optically active defects has been observed in diamond establishing this material as a promising platform for exploring properties at the quantum scale. Nevertheless, the search for new defect centres [33,34] and the identification of centres of unknown nature is an ongoing topic. It is of particular importance to develop procedures allowing reliably controlling the formation of those defects which usually have reproducibility issues. The aim of this study is to “screen” the periodic table of elements by implantation and annealing and help retrieve or discover optical centres in diamond in a systematic manner. Wide-field optical characterisation methods were employed at first and then confocal microscopy and spectroscopy, as well as sub-diffraction methods in some special cases.

One of the main challenges regarding quantum applications based on optical centres in diamond concerns the reproducibilty of the diamond substrates and of the optical centres environment. Quality control at the quantum level should be considered and developed. That is for example fluorescence stability but also charge state control, as well as spin coherence time. All these properties and parameters can be investigated by taking advantage of the long experience gained from the NV centres that can be exploited to locally probe the material quality and the local environment of the optical centres that we aim to screen.

In this paper, we will first present the fabrication method used to search and create optical centres with high throughput. We will briefly recall the ion-matter interactions and discuss the main implantation defects, illustrated by experimental results, and the effects of thermal annealing. We will then estimate the diffusion coefficient of nitrogen, vacancies, carbon interstitial and hydrogen, which are the main species found in an implanted CVD diamond. A short section will be dedicated to diamond homogeneity and quality control of the samples and the created centres. In the last part, we will present the first results of our screening method and discuss the properties of some of the newly found fluorescent centres.

1 Method for the ion implantation screening of different chemical elements

In this first section, the screening of optical centres in diamond by ion implantation will be presented. Ion implantation is the method of choice for a high throughput screening of different chemical elements. The advantages are: the possibility to select an atom (also the isotope) or molecule and to implant it with high spatial resolution and in a countable way [35-37], even deterministically [38,39]. However, it induces defects which require an optimised thermal annealing to heal them out. Chemical vapour deposition (CVD) also enables the creation of some optical centres during the growth (NV, SiV,

GeV), with generally better overall properties but without the possibility to screen many elements or place them on demand [40,41]. Due to the compact carbon lattice, large atoms cannot be easily accommodated by direct growth in the film. Phosphorous has for instance a very low doping efficiency especially on a (100) orientation [42,43]. This explains that only relatively light elements are routinely in situ doped so far. Moreover, the spatial localisation of the dopants during CVD growth is further complicated by memory effects or long gas residence times that do not allow obtaining easily abrupt doping profiles. For these reasons, the screening of colour centres through an implantation procedure appears as a more reliable way to produce specific defect centres.

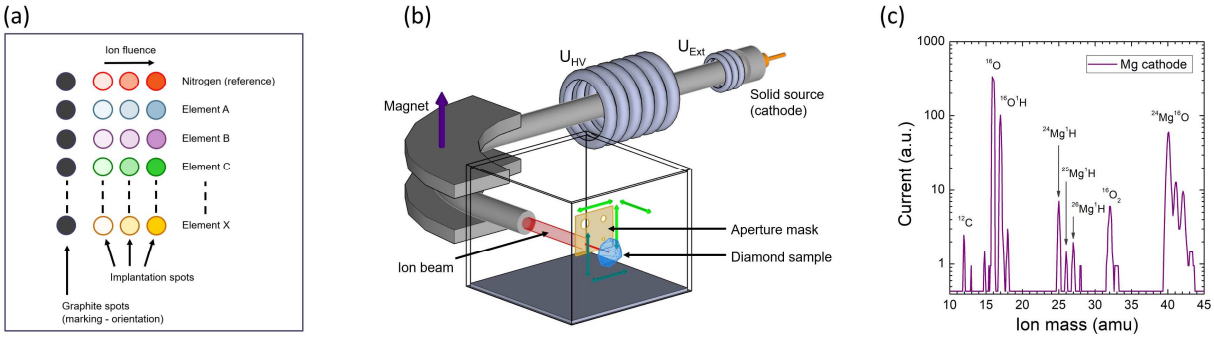

Figure 1. Colour centre screening in diamond. (a) Scheme of a diamond sample implanted in a systematic manner with a series of chemical elements. Graphite spots are pre-implanted (by ion-beam induced amorphisation followed by thermal annealing) for marking and orientation. Nitrogen spots are implanted to use NV centres (or H3 centres) as reference and quality control. The sample will further be annealed at different temperature steps to study the building and stability of the different defect centres. (b) Scheme of the 100 kV ion accelerator, showing the easily changeable source cathode, the extraction and acceleration high voltage units, the electromagnet for mass and isotope selection, the aperture system (mounted on a xyz) and the sample stage. (c) Typical mass spectrum of a (here magnesium) home-made cathode used in the following and measured at the sample position. The main peaks are labeled with the corresponding elements.

The systematic study we are following here relies on ion implantation only. An ion accelerator can provide different ion species (atomic or molecular) and mass selection of the different isotopes is easily done. The choice of the ion kinetic energy ensures the control of the penetration depth. With the use of a focused beam and optical system, it is possible, without lithography, to "pattern" a periodic system of elements into a diamond sample, as illustrated in Figure 1a. In the following, the 100 kV accelerator of the University Leipzig is used to provide a large range of ion species, suitable for the high-throughput screening of optical centres in diamond. The ion accelerator (Figure 1b) consists of a Cesium sputter source in which home-made cathodes of different chemical composition can be mounted. With this setup, only negative ion species are available. More details can be found in [44]. A 90° bending electro-magnet is used for the mass selection of the desired ion species. A typical mass spectrum is shown in Figure 1c, for a magnesium cathode. The different peaks are well separated which ensures a pure isotopic content for each ion species implantation. The ion beam is then focused on the target using an in-situ masking system consisting of apertures of different sizes. The selected ion species can therefore be precisely implanted at different positions on the diamond sample as schemed in Figure 1a. For alignment and orientation, the sample is pre-patterned with graphite spots. This is easily done also with the ion beam, implanting a spot with an ion fluence above the graphitisation threshold of about 10^{22} vacancies / cm^3 [45]. After annealing, the damaged regions with defect densities exceeding this value will be transformed into graphite, and become visible under optical microscope.

2 Interaction of ions with matter

2.1 Defect production and ion channeling

The main interaction of kinetic ions with matter is an interaction with the electrons of the crystal atoms. The Coulomb interaction can be calculated by the Bethe-Bloch formula and is theoretically and experimentally well understood. The energy transfer to the electrons depends on the kinetic energy and the mass of the ions. For the ion energies used in the following (of up to a hundred keV), the typical energy gained by the electrons is too low to displace a crystal atom. The energy transfer is also too low to significantly heat up the ion path and no displacement takes place at all by the interaction with electrons. The heating of the sample needs to be taken into account only for high ion currents, but it negligible in the following. However, the interaction of the ions with the electrons leads to a slowing down of the ions which is called electronic stopping.

Defects occur only in a direct interaction of the kinetic ions with the nuclei of the crystal atoms (so-called nuclear stopping). This process takes place most efficiently at low energy of the ion (below a few tens of keV) and leads to the displacement of an atom if the kinetic energy transfer exceeds the displacement energy of the bound atom. The typical displacement energy for diamond is 40 eV. Additionally, the displaced atom can itself interact with other crystal atoms and further displace them. This effect results in a cascade of displaced atoms (see Figure 2c). SRIM simulations [SRIM] allow to calculate the number of vacancies produced by the implantation of an ion into a solid and take secondary displacements into account. The program assumes a random distribution of the crystal atoms and achieves very good results if the ion beam direction is tilted a few degrees out of one of the main crystal axes. The program only calculates the interaction of the ion and no annealing of the crystal. An additional source of mistake will be induced if the direction of the incident ion is small with respect to the crystal lattice; ion channeling can then take place. In this case, the ion can travel through atoms rows or planes as guided by the electric potential, generally penetrating deeper and producing a different defect distribution along the depth [46]. This is important to consider when a high precision placement of the optical centres is required. This effect is well described in silicon [47] and it was also observed in diamond implantations [37,48-50]. It can be modeled using the CTRIM code [51], as illustrated in the following with the example of 4 keV nitrogen, which is often used to produce shallow NV centres for magnetometry. Figure 2a shows CTRIM simulations of the vacancy depth distribution (upper graph), calculated for two incidence angles of 0° and 7° with respect to a perfectly flat (001) surface. The lower graph is a plot of the depth distribution of the implanted nitrogen atom. It can be seen that channeling leads to different depth profiles both for the nitrogen and the vacancies. Indeed, the ion channeling (and amount of ions effectively channeled) depends at first on the incidence angle with respect to a given channeling direction, but also on many parameters such as the ion energy, ion species, target material, crystal orientation or beam divergence. But it also strongly depends on the surface roughness which is a parameter difficult to evaluate and poorly reproducible. We found that the experimental implantation impurity profiles found in [37] and [49] (measured by Secondary Ion Mass Spectrometry, SIMS) cannot be fitted without introducing a surface “roughness” in the simulation. This has been done in the results presented in Figure 2b. Here, a 1.5 nm layer of amorphous carbon was introduced to account for the surface roughness. It can be seen that the channeling effect is strongly reduced. This is supported by the atomic probe tomography results conducted on diamond implanted with 5 keV nitrogen at vertical incidence onto a (111) surface [52]. However, it is important to consider the surrounding defect configuration at the end of range where the ion finally stops within the crystal lattice, in both cases of channeled and not channeled ions. In order to study this more precisely, we have conducted molecular dynamics [53] simulations of the implantation of 4 keV nitrogen at 0° and 7° incidence onto (100) diamond. The development of the ensuing collision cascade was followed for 3 ps, which was found to be a sufficiently long time for the collision cascade to cool down and athermal defect recombination process to stop. Naturally, within this time scale practically no defect migration driven by equilibrium thermal activation can take place.

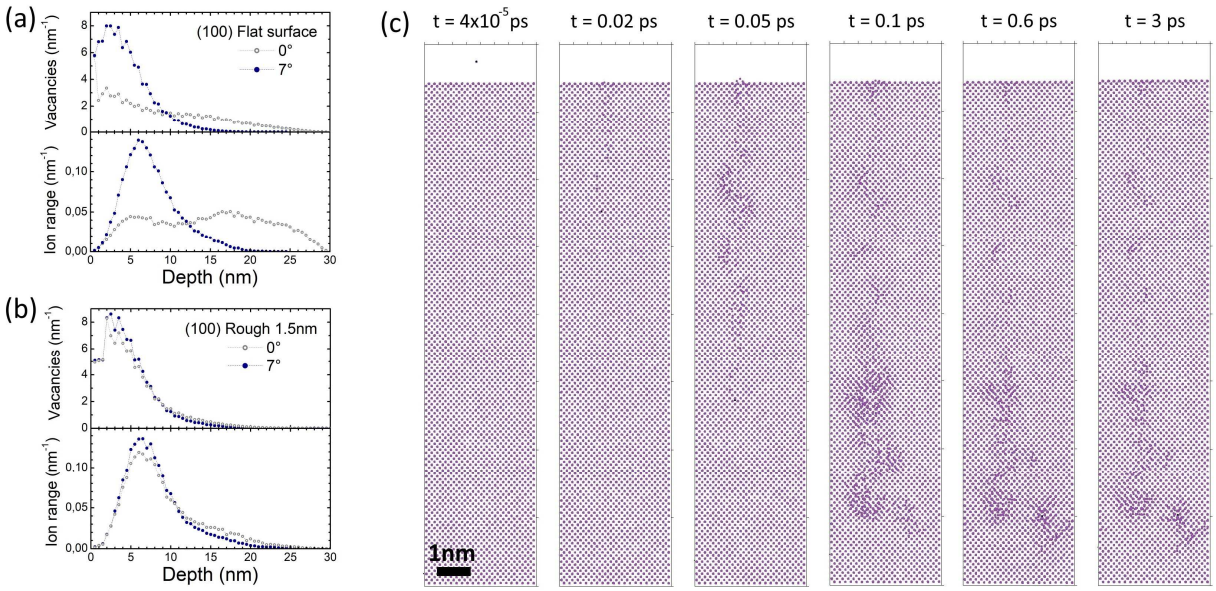

Figure 2. (a) CTRIM simulations of 4 keV nitrogen implantation into (100) diamond with perfectly flat surface, at the different incidence angles of 0° and 7°. The upper graph shows the vacancy depth profile and the lower graph the ion distribution (simulation done with 50000 ions). (b) Same simulations in the case of a (100) surface having a roughness of 1.5 nm. This is done by adding a top layer of amorphous carbon of 1.5 nm thickness. (c) Snapshots of atom positions from an MD simulation of a 4 keV Nitrogen impact (dark circle) on Carbon (light circles). All atoms in a region of 3.6 nm lateral size in both the *x* and *y* coordinates and 15 nm deep in *z* are shown: since the sample is crystalline, it is possible to "see" through the crystal, so that the defects that are on off-lattice positions are clearly visible. The diamond lattice, with a (100) surface normal, was first equilibrated at 300K for 1 – 3 ps to give the atoms realistic thermal displacements and allow for surface relaxation. The well-tested Brenner potential [54,55] was used to simulate the C atom interactions, while the N-C interactions were described with a dimer pair potential [56].

After defect analysis, we also calculated the distance from the N atom to the nearest vacancy, and made statistics of how many vacancies and interstitial were within 1 nm of the final N atom position (the interstitial formed by the N atom itself was not counted in this statistic). The snapshots of a typical event are illustrated in Figure 2c. Most of the primary damage is in small disordered atom regions, rather than isolated point defects. In a clear majority of cases, the final position of the N atom was within such a disordered cluster. In only one case out of ten off-normal impact cases simulated, and none out of the ten normal impact cases, was the final N atom separated by more than 1 nm from all intrinsic defects. The MD simulation results on the damage production show that in the primary damage state after a cascade has cooled (at 3 ps, before any thermal defect migration) the implanted N is in most cases surrounded by closeby vacancies and interstitials, or in other words part of a damage pocket. What is important to note is that the difference between the implantations into channeled and non-channeled directions is minor. Note that all the implantations conducted in the following sections were done on (100) diamond at 0° incidence where channeling likely occurs.

2.2 Characterisation of implantation defects

It is not the purpose of this work to review all the radiation defects, however it will be focused on some of them and on specific aspects which are of relevance for the creation and application of single optical centres in diamond for quantum based applications. Indeed, the use of single centres in diamond for quantum purposes imposes some requirements on the local environment of the defects. Most of the experimental demonstrations were achieved using the NV centre, which was historically seen as the most promising qubit in the solid state. Its unique optical and spin properties proved to be extremely suitable for sensing, especially using the coherence properties of single NV^- centres. That can be therefore used in our screening purposes, as a witness for other defect centres.

It is inherent to any implantation that radiation defects are produced, at first carbon interstitials and carbon vacancies, but also more complex intrinsic defects. The major problem of the ion implantation technique for quantum applications or electrical doping remains in the fact that all the radiation defects due to the ion implantation process cannot be totally annealed out. Many studies deal with this problem, however mostly on ensembles with large numbers of defect centres. It was only recently that this topic could be brought to defects at the single level. Especially, the comparison between NV centres obtained by nitrogen implantation and annealing or by nitrogen doping during a CVD growth process showed that the coherence times of the native grown NV centres was generally better than for the implanted ones [41,57], revealing a better environment. It is therefore of high importance to know, control and engineer the local environment of the defect centres that we aim to produce. For example, considering the defect family of column IV elements associated with a split vacancy (SiV, GeV, SnV and PbV centres), the vacancy configuration after implantation is expected to vary strongly due to the different masses of these atoms. This is what we will consider in the next section. Attempts to create PbV centres are still ongoing. One of the possible reasons that it was not observed yet lies in the very different atomic mass between Si and Pb, not only from the crystalline point of view, but also from the implantation defects.

2.2.1 GR1 centres (single neutral vacancies)

The most prominent NV and SiV centres involve vacancies and we discuss here first the production and measurement of single vacancies. Especially, we focus here on the GR1 (V^0, neutral vacancy) centre, with a characteristic ZPL at 741 nm [1], which can be easily observed with a confocal microscope. A simple experiment can be conducted, which consists in measuring the vacancy production depending on the mass of the implanted ion (for similar penetration depth and fluence). Figure 3a is a collection of confocal fluorescence scans recorded directly after the ion implantation (without annealing) of ten different elements, at the same ion fluence of 1×10^{12} cm^{-2}. A long pass filter (650 nm) is used to suppress the diamond Raman line and select the fluorescence of the GR1 defect. The corresponding fluorescence spectra of four elements (Li, Mg, K and Sr) are plotted in Figure 3b. Interestingly, we see that the fluorescence intensity of the GR1 decreases when the atomic mass is increased (Figure 3d, orange dots). This is a rather counter-intuitive observation because a heavier ion produces more vacancies than a lighter one, as illustrated in Figure 3d (blue stars) from a SRIM simulation [58]. A 2D simulation plot of the vacancy distribution for Li, Mg and Sr is however shown in Figure 3c. It illustrates that lighter ions tend to produce more isolated vacancies whereas, for heavier ones, much higher vacancy densities are reached along the ion path. Therefore, it is believed that vacancies form complex [59] or disordered clusters (as seen in the MD simulation of figure 2a) in the case of heavier ions which explains the observed fluorescence quenching (as already reported on NV centres [60,61]). This highlights the fact that very different defect distributions do surround implanted atoms of different masses such as N, Si, Ge, Sn or Pb, possibly leading to multiple complex configurations. For example, the creation efficiency of NV centres is highly dependent on the energy of the nitrogen atoms [60], as it will be recalled in Figure 6b. Furthermore, by looking in details at the K and Ca implantation spots, even though the fluence of 1×10^{12} cm^{-2} is moderate, we observe a “dosis” nonlinear effect on the GR1 emission: the centre of the spot is darker than the edge (illustrating the non-uniform implantation fluence which is maximal at the centre). The GR1 fluorescence decreases while the fluence increases. Not only the mass of the ion, but this dosis effect indicates that there is a possible overlap between the vacancy “clouds” produced by each ion and that, again, the fluorescence starts to be quenched or that more complex defects build. The corresponding vacancy concentration for these K and Ca implantations is locally about 7×10^{19} cm^{-3}, still at least two orders of magnitude below the graphitisation threshold, but with an average V-V distance of about 2.4 nm. For the Mg spot, which does not show such this effect, the average V-V distance is about 3.06 nm. It is therefore an effect with a sharp threshold transition, which may give insights in the vacancy formation and mobility during the ion implantation process. This threshold density of vacancies (V-V slightly below 3 nm) when the quenching of the GR1 fluorescence starts has also been found using carbon implantations of different fluences (not shown).

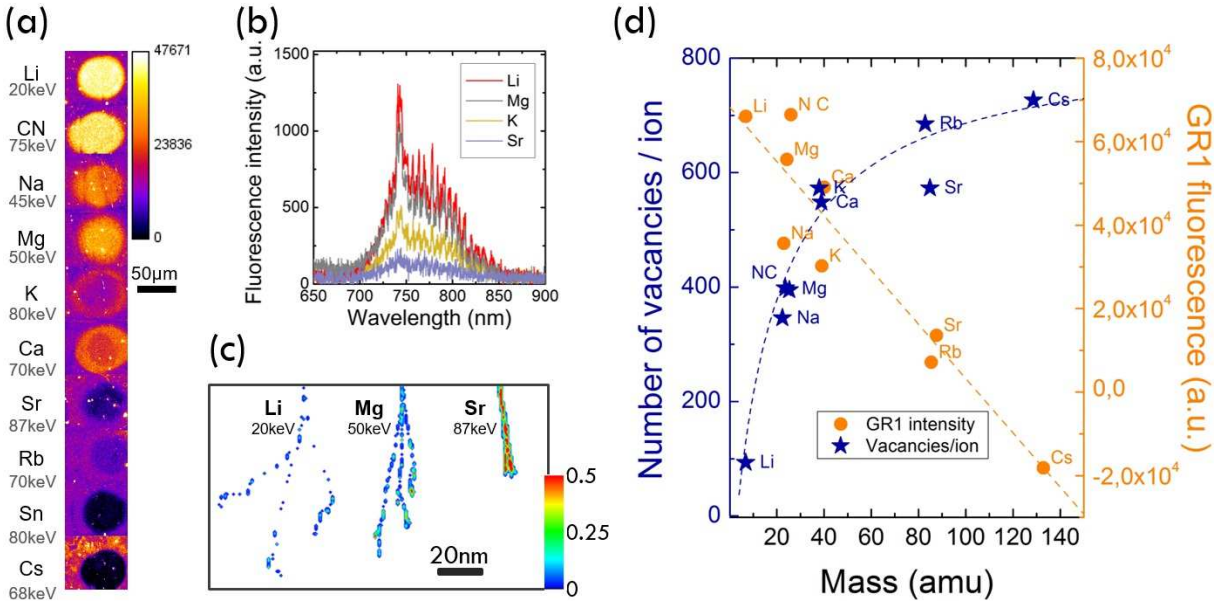

Figure 3. Ion implantation related defects: GR1 centres. (a) Confocal fluorescence scans of an "electronic grade" diamond implanted with different ion species of increasing mass (but at the same ion fluence of 1×10^{12} cm^{-2} and comparable penetration depth of 50 to 70 nm). The laser excitation is 532 nm and the fluorescence is filtered with a longpass filter 650 nm to image the neutral single vacancies (GR1). (b) Fluorescence spectra of the Li, Mg, K and Sr implantations. The spectra were recorded by scanning a 10×10 µm² area at the centre of the implantation spots and subtracting it with the reference spectrum from a 10×10 µm² unimplanted area taken apart. (c) SRIM simulation for three elements Li, Mg and Sr, showing the vacancy density distribution produced by the implantation of three ions of each ion species. The unit is given in vacancies / nm². (d) Plot of the number of vacancies produced per implanted ion, simulated with SRIM (blue stars) and of the measured GR1 fluorescence intensity (orange dots) as a function of the ion mass.

2.2.2 3H centres (double carbon interstitial)

Another well-known and optically active radiation defect is the 3H centre, with a ZPL at 504 nm. It is attributed to <100> split self-interstitial [1,62,63]. The 3H centre generally efficiently forms above temperatures of 300°C to 400°C and anneals out at different temperatures depending on factors such as the nitrogen concentration or the doping level. Figure 4a is an optical widefield fluorescence image of an area of the screened diamond implanted with Na, Mg, K, Rb and Cs and annealed 4 hours at 600°C in vacuum. The green fluorescence of the 3H centres is visible for the highest fluence spots of the three heaviest atoms. A fluorescence spectrum from the Cs spot is plotted in Figure 4b. In contrast to the GR1 centres, it can be seen here that the intensity of the 3H centre increases with the ion mass (inset in Figure 4b). Besides, a green corona of 3H centres is also present around each graphite spot. During the implantation process, the ion beam is slightly scattered at the masking aperture, leading to a tail around each spot, having a decreasing fluence with increasing distance from the centre of the spot. There is however again a nonlinear fluence dependence : the 3H fluorescence intensity is maximum within a narrow fluence range as indicated by the relatively sharp edges of the fluorescence and decreases in the centre of the spot. The evolution of the 3H signal on the temperature range is shown in Figure 6a.

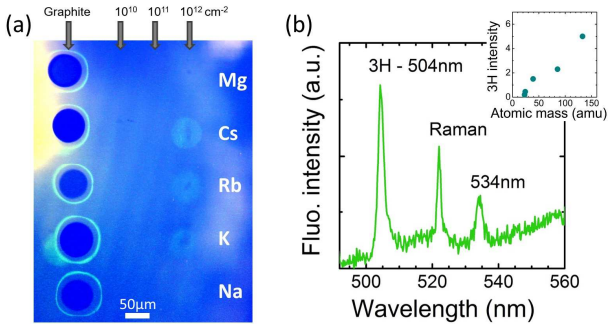

Figure 4. Ion implantation related defects: 3H centres. (a) Widefield fluorescence image of a 550 × 700 µm² area of a screened diamond with Na, Mg, K, Rb and Cs ion implantation, recorded after annealing at 600°C for 4 hours. The fluences are 1×10^{10} cm^{-2}, 1×10^{11} cm^{-2} and 1×10^{12} cm^{-2}. The excitation wavelength is 488 nm. The five reference graphite spots can be recognised. A weak and green fluorescence can be seen from the heaviest ions at the highest fluence and corresponds to 3H emission as well as the halos around the graphite spots. (b) Fluorescence spectrum of 3H centres taken from the Cs spot. The inset shows the 3H intensity as a function of the ion mass, for the 1×10^{12} cm^{-2} fluence. The corresponding implantation energies are indicated in Figure 2a.

2.2.3 The 2.807 eV and 3.188 eV centres

These two defect centres are often observed together after ion implantation processes in diamond. They are believed to be related to nitrogen and interstitial carbon atoms [1,64]. They present a ZPL at 441 nm (2.807 eV) and 389 nm (3.188 eV) respectively, accompanied with a significant phonon sideband. We have prepared a sample (ultrapure CVD growth of ≈ 100 µm on top of a (100) HPHT substrate) with a set of nitrogen implantations at different ion energies (0.8 keV to 5 keV) and ion fluences (10^9 cm^{-2} to 10^{13} cm^{-2}). The sample was annealed at 800°C for 2 hours in vacuum to form NV centres and to check the appearance of the 2.807 eV and 3.188 eV defect lines. It was characterised by standard confocal scanning fluorescence microscopy for imaging and spectroscopy of the NV centres (laser excitation 532 nm, detection with a bandpass filter 660 nm – 735 nm) and by cathodoluminescence (CL).

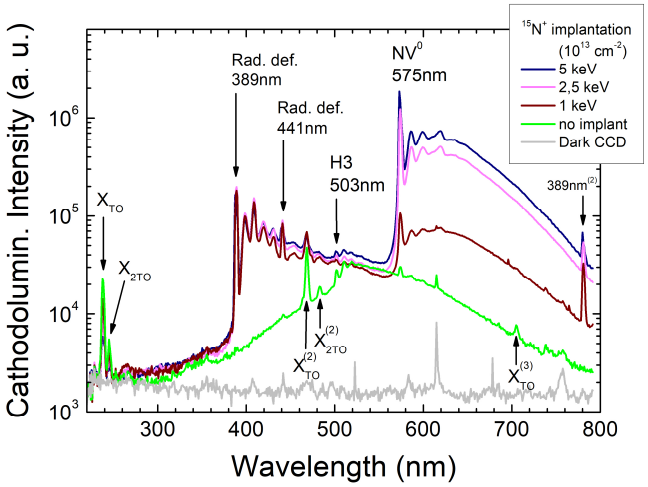

Figure 5. Cathodoluminescence spectra at 85K of three of the nitrogen implantations (energy of 5.0, 2.5 and 1.0 keV, fluence of 1×10^{13} cm^{-2}), measured with an electron beam of 5 keV energy and xx pA. The spectra are dominated by the NV centres. The radiation defects at 389 nm and 441 nm are also present. The spectra of the unimplanted diamond and of the CCD dark counts are also plotted for comparison.

The CL fluorescence spectra recorded at T = 85K from 3 different implantation spots (energies of 5, 2.5 and 1 keV and same fluence of 10^{13} cm^{-2}) and from the unimplanted diamond are plotted in Figure 5. As expected, the spectra are dominated by the emission of the NV centres. Note that only the contribution from the neutral charge state NV^0 with a ZPL at 575 nm (and not from the NV^-, ZPL at 638 nm) is present, as already observed in CL [1] and EL with pin diodes [65,66]. Note also that the ion energy dependence of NV centre creation yield is here again observed as in [60] (see also Figure 6b).

The 3.188 eV defect (389 nm) together with its characteristic phonon sideband can be seen and is therefore not annealed out at 800°C. It has the same intensity for the 3 implantations and therefore does not appear to have any ion-energy dependence. The emission is only one order of magnitude weaker than the NV centre at 5 keV (about 5×10^{11} NV/cm^2) however it is of comparable intensity with the NV centres implanted at 1 keV. As well, the 2.807 eV defect (441 nm) together with its phonon sideband is visible but with a weaker intensity than the 3.188 eV defect. It can be seen that its intensity increases with the ion energy, like the NV centres emission does, however not as strongly. The observation of the 3.188 eV and 2.807 eV defects under nitrogen implantation and 800°C annealing is in agreement with the proposed nature found in [1,64] of a nitrogen atom and carbon interstitial. It will be of interest to follow their temperature behavior at different implantation fluences in further studies. Furthermore, there is a peak at 470 nm which points out at the emission wavelength of the TR12 centre, another often observed radiation defect [1,67]. However, it is believed that it is the replica of the free exciton emission (noted X_{2nd}), because it is also present in the unimplanted region. Interestingly, no signal from the GR1 or the 3H centres can be found, although the implantation fluence was relatively high. This indicates that they have likely annealed out or are present as vacancy complexes (the sample was annealed only to 800°C). Note the very weak contribution from H3 centres (involving two nitrogen atoms, ZPL at 503 nm) which is expected to arise from the bulk substrate.

3 Thermal treatment

As discussed above, different kinds of defects can form depending on the implantation energy and fluence or doping level in the diamond. It is also relevant to estimate the influence of the annealing treatment on the colour centres formation. The best example of this is nitrogen. The classification of diamond was historically made out of whether nitrogen is present (type I) or not (type II) and in which form: type Ia (no nitrogen impurities), type IaA (aggregated nitrogen pairs), type IaB (aggregated 4N + V) and type Ib (isolated nitrogen). Thermal (and pressure) treatments are widely used in jewelry in order to change the colour or glance of gemstones and increase their commercial value [68]. The first goal of a thermal treatment after any ion implantation process is however to heal the radiation defects as good as possible. Our aim for the screening study is furthermore to perform different annealing steps and to characterise the implanted areas after each of these steps in order to follow the defect production evolution related to each implanted element. Several optically active radiation defects such as the ones presented above (GR1, 3H, 3.188eV and 2.807eV) can be followed to control the healing process. In addition, we will use for example the dissociation of NV centres into H3 (N-V-N) centres to estimate the diffusion coefficient of nitrogen at a given temperature.

3.1 Diffusion of vacancies

The creation of NV centres by nitrogen ion implantation requires an annealing step to ensure the positioning of the nitrogen atom in a substitutional place and the diffusion of vacancies (produced by the kinetic nitrogen ion along its path) until one of them is captured to form the NV centre. The efficiency of this statistical process is often given as the NV creation yield (number of observed NV centres with respect to the number of implanted nitrogen atoms). It depends mainly on the annealing temperature [1,60] and on the implantation energy [60]. The typical “yield vs energy” dependence is plotted in Figure 6b for two different samples of high purity. It shows that the yield is in the percent range only at energies of a few keV, to produce shallow NV centres (a few nm depth). The use of such low energies is necessary for application like magnetometry [12] (sensitivity proportional to $(1/d^3)$ where d is the NV-object distance) or high spatial resolution implantation (to avoid ion straggling into the material) [69]. Therefore, in the last years, efforts were done to improve the NV creation yield [70-73] and to understand better the mechanisms in play. The annealing temperature (or time) necessary to form the NV centres needs to be sufficient so that the vacancies become mobile. A double exponential behaviour is generally observed in the annealing out of vacancies: due typically to the recombination of vacancies and carbon interstitial starting at 600°C, and to the diffusion of vacancies becoming significant at about 800°C [74]. In Figure 6a, the temperature dependence of the NV fluorescence is plotted as a function of the annealing temperature for two different ion fluences (10^{13}

cm^{-2} orange dots, 10^{15} cm^{-2} red dots) of N implantation into two type-IIa diamond samples. At temperatures around 1000°C, a plateau is reached and when the temperature is further increased, the NV centres tend to dissociate and possibly form other defects. This is supported by Figure 6c, showing the fluorescence decrease as a function of time from an ensemble of implanted NV centres heated at 1600°C. Interestingly, we found that a same thermal treatment at 1600°C applied to electronic grade diamonds with [N] < 1 ppb also induces NV centres to form however from the native nitrogen. This was measured several times and is shown in Figure 6d for a sample from which no single NV could be found before the 1600°C treatment. The dispersed bright spots in the scan are single NV centres which can be found within the whole diamond (with an average distance of 1 to 5 µm, corresponding to an NV density of 10^{10} to 10^{12} cm^{-3}). This effect cannot be observed in optical grade material due to the too large amount of native nitrogen and NV centres already present. A possible explanation would be that the diffusion length of the native vacancies present in the diamond became large enough to enable them to "reach" a native nitrogen.

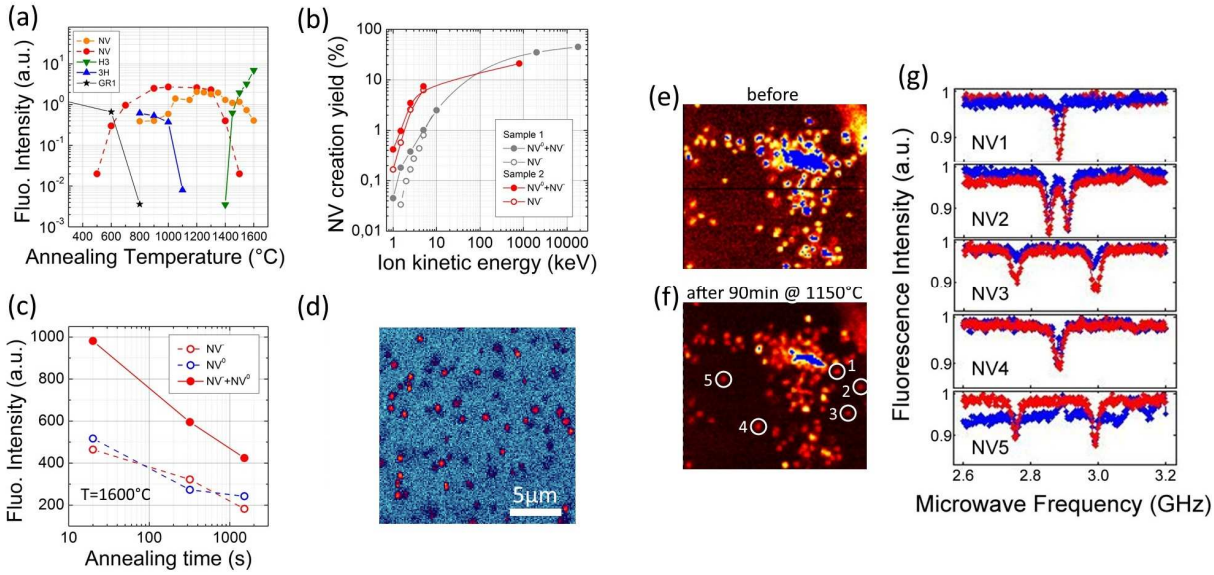

Figure 6. Thermal stability and creation yield of NV centres. (a) Fluorescence intensity vs annealing temperature of different defects: NV, H3, GR1 and 3H. The NV centres correspond to implantations of nitrogen at 45 keV and 1×10^{15} cm^{-2} (orange dots) and to 300 keV and 1×10^{13} cm^{-2} (red dots). (b) NV centre creation yield vs ion implantation energy for two different samples annealed at 800°C in vacuum for 2 hours. The hollow circles account for the NV^- fluorescence (using a longpass 650 nm filter) and the filled circles for the NV^0 + NV^- fluorescence. (c) NV fluorescence vs annealing time at a temperature of 1600°C in vacuum, measured from an implanted area with 45 keV nitrogen ions at the fluence of 1×10^{15} cm^{-2}. (d) Fluorescence confocal scan of an "electronic grade" samples annealed 4 hours at 1600°C in vacuum. Although no single NV is found before annealing, the thermal treatment induces the formation of single NV centres at a density of about 0,1 – 1 NV / µm². (e) Confocal fluorescence scan of a low-fluence implanted diamond with 5 keV nitrogen, after a 2 hours annealing at 900°C. (f) Scan of the same region after a 90 min annealing at 1150°C. Almost none of the about 200 NV centres has disappeared. (g) Optically detected magnetic resonance (ODMR) spectra of 5 single NV centres recorded before (red) and after (blue) the 1150°C treatment. A weak magnetic field is applied in order to distinguish between the 4 different possible orientations of NV centres due to different Zeeman splittings. At least four of the five studied NV centres did not change the orientation of the NV bond during the thermal treatment.

Not only the creation yield is important, but the removal of all the surrounding implantation defects is a key issue for quantum applications based on the spin of the NV^- centre. It was shown in ref [59] that the most suitable annealing temperature to remove paramagnetic defects is about 1100°C. At such a temperature, most of the $(V_n)^0$ defects anneal out, which can be followed by measuring the coherence time of single NV centres [59]. In this context, we have checked the stability of single NV centres at a slightly higher temperature of 1150°C. This experiment is based on confocal imaging of single NV

centres and on ODMR spectra to check whether the vacancy moves around the nitrogen atom, possibly leading to a new orientation of the NV centre within the diamond crystal. This can be followed by applying a low magnetic field and measuring the Zeeman splitting between the two resonances between the $m_s = 0$ and $m_s = \pm 1$. For a misaligned B field, each of the four [111] possible orientations of NV centres will give a different Zeeman splitting. The first test consisted in imaging an area of a diamond randomly implanted with 5 keV nitrogen (Figure 6e). The same zone was then imaged again (Figure 6f) after a 90 minutes annealing at 1150°C in vacuum. It can be seen that none of the about 200 single NV centres has disappeared. No additional NV has neither appeared. At the scale of the optical setup, it seems that no diffusion of the NV as a whole happened. To look further whether the vacancy may have changed place about the nitrogen atom, 5 single NV centres were selected and their ODMR spectra were taken before and after this 90 minutes thermal treatment. The results are plotted in Figure 6g. The orientation of four NV centres is the same, whereas it cannot be concluded about NV5. What is important to note here, is that the NV centres are extremely stable at 1100°C which is the most suitable temperature to remove as many vacancy complexes as possible and to obtain the best coherence times.

The increase of the NV yield with increasing implantation energy shown in Figure 6b is always observed. It can be explained by the number of vacancies per ion which increases with the ion energy (and therefore the probability to build a N-V complex during annealing) together with the increased probability to lose vacancies at the diamond surface. Moreover, due to surface proximity and band bending, a significant amount of the very shallow NV centres may be present in the NV^+ charge state which is optically inactive, reducing the apparent NV yield. This is supported by the increasing NV^0/NV^- ratio observed for both samples in Figure 6b when the implantation energy is reduced below 5 keV. Note that it was shown in [71] that a p-type doped layer leads to charge single vacancies positively as V^+, which in turn, precludes the formation of di-vacancies by Coulomb repulsion. Neutral single vacancies can more easily form di-vacancies, which are more difficult to anneal out and which do not contribute to the formation of NV centres.

The presence of water at the diamond surface during annealing, which can provide hydrogen species by breaking of the water molecule might also lead to a lower yield for very shallow NV centres. Besides, hydrogen diffusion is known to induce passivation of NV centres by the formation of stable NVH complexes (only visible in electron paramagnetic resonance (EPR) or Fourier transform infrared spectroscopy (FTIR) depending on its charge state) and we will discuss it in the following.

3.2 Diffusion of Nitrogen atoms

The very low diffusion of impurities in diamond makes it difficult to precisely estimate it experimentally. In the case of diamonds in which nitrogen is the dominant impurity (in the range 100 ppb to several ppm), the relative amount of NV and H3 centres can be however used to estimate nitrogen diffusion at the nanometer scale. Indeed, with increasing temperature, nitrogen atoms tend to aggregate and build more complex defects [75]. We can use this effect to determine the diffusion coefficient of nitrogen following the fluorescence of both of these defects in a simple experiment. In this purpose, we implanted different areas of an “optical grade” quality diamond from element 6 with nitrogen ions, at fluences between 10^{12} cm^{-2} and 10^{15} cm^{-2}, and set the kinetic energy to 45 keV (average depth of 60 nm). The corresponding local nitrogen densities are in the range 2×10^{17} cm^{-3} to 2×10^{20} cm^{-3}, which in turns correspond to average closest nitrogen-nitrogen distances in the range 17 nm to 1.7 nm. Subsequently, the diamond was annealed in vacuum at increasing temperatures from 500°C to 1600°C (see Figure 6a), staying about 20 seconds at each target temperature. Afterwards, the sample was heated further at 1600°C for a total annealing time of 320 seconds and 1520 seconds respectively. The fluorescence intensities of the NV and H3 centres were then studied as a function of annealing temperature and annealing time using a confocal microscope. For the 10^{13} cm^{-2} fluence (Figure 7a) only NV centres are observed, whatever the annealing temperature during this time. In such conditions, the 7.9 nm N-N distance is too large to enable the building of H3 centres. For the 10^{14} cm^{-2} fluence (Figure 7b), the spectral signature of the H3 centres appears for the highest treatment temperature of 1600°C, indicating that some nitrogen diffused as far as the closest nitrogen atom, expected to be here 3.7 nm apart. To analyse these spectra, the reference emission spectra of single

H3, NV^0 and NV^- centres (Figure 7d) were used. The temperature dependence of the fluorescence of the NV and H3 centres is presented in Figure 7e. The time dependence of the NV/H3 ratio was studied for the highest temperature of 1600°C. The fluorescence spectra presented in Figure 7c (fluence of 10^{15} cm^{-2}) reveal that most of the implanted NV centres have disappeared and that the H3 centres became the dominant species after 1520 seconds at this temperature.

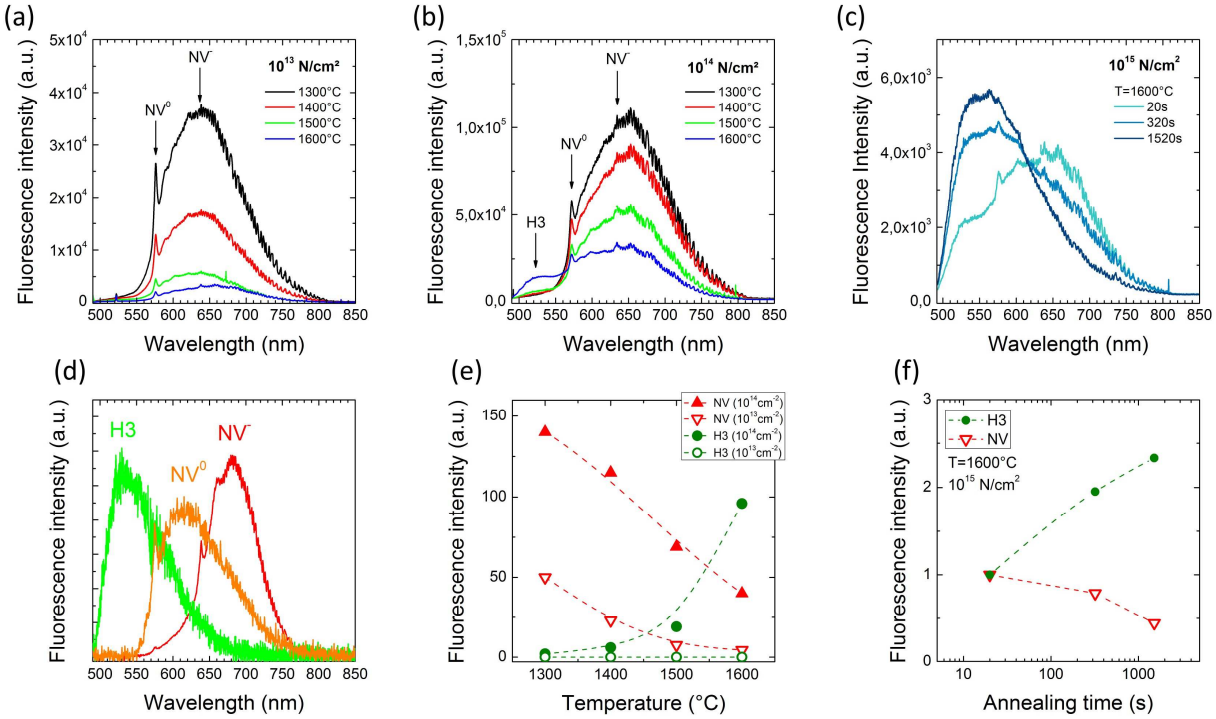

Figure 7. Nitrogen diffusion revealed by the evolution of the NV/H3 ratio. (a) Fluorescence spectra of a nitrogen implantation at the fluence of 1×10^{13} cm^{-2}, recorded after different thermal treatments between 1300°C and 1600°C. (b) Fluorescence spectra of a nitrogen implanted region with a 10 times higher fluence (1×10^{14} cm^{-2}) recorded after different thermal treatments between 1300°C and 1600°C. (c) Fluorescence spectra of a highly nitrogen implanted region (1×10^{15} cm^{-2}) recorded after different annealing times of 20, 320 and 1520 seconds, at a temperature of 1600°C under vacuum. (d) Reference spectra of H3, NV^0 and NV^- used for fitting the data. (e) Fluorescence intensity vs annealing temperature for the NV and H3 centres. (e) Fluorescence intensity vs annealing time at 1600°C for the NV and H3 centres.

As well, this is shown in figure 7f, where the NV and H3 fluorescence were normalised to their respective fluorescence after the 20 seconds annealing at 1600°C. Assuming that the diffusion length is now roughly equal to the average distance between the implanted nitrogen atoms at this fluence of 10^{15} cm^{-2}, which is about 1.7 nm, we can estimate the diffusion coefficient of nitrogen. Using Fick´s second law of diffusion

$$\frac{\partial C(\vec{r},t)}{\partial t} = D\,\nabla^2 C(\vec{r},t)$$

where $C(\vec{r},t)$ is the nitrogen concentration, in one dimension the diffusion coefficient D can be estimated to be

$$D = \frac{x^2}{t} = 1.7\times10^{-17}\ cm^2/s$$

This is supported by the results in Figure 7a and 7b, which show that at the 10 times lower fluence of 10^{14} cm^{-2}, some H3 centres appear, while none of them is formed at 10^{13} cm^{-2}.

3.3 Diffusion of Hydrogen – passivation of NV centres

Hydrogen is likely the most common impurity in high purity CVD diamonds (with boron and nitrogen concentrations of a few 10^{14} cm^{-3} or less) due to the use of hydrogen plasma for the growth. It is however difficult to estimate the total hydrogen concentration. Methods such as secondary ion mass

spectroscopy (SIMS) or nuclear reaction analysis (NRA) have both typically ppm sensitivity for hydrogen, limiting the lowest measurable concentration to ≈ 10^{17} cm^{-3} [76]. The [H] concentration may depend on the growth conditions such as the temperature, pressure, growth rate or crystal orientation. Nevertheless, it can be estimated indirectly through its involvement in many known defects (and possible important role in their formation). For example, the NVH concentration can be estimated by EPR (NVH^-) or FTIR experiments (NVH^0) [77] and compared to the concentration of substitutional nitrogen and NV centres. Besides, it is known that the V-H and impurity-V-H complexes are very stable [78]. As a consequence, it is important to take hydrogen diffusion into account when aiming at the creation and use of optical centres in CVD diamond. Reversibly, the study of optical centres and their temperature behavior may be a way to have better insights into the hydrogen concentration and homogeneity.

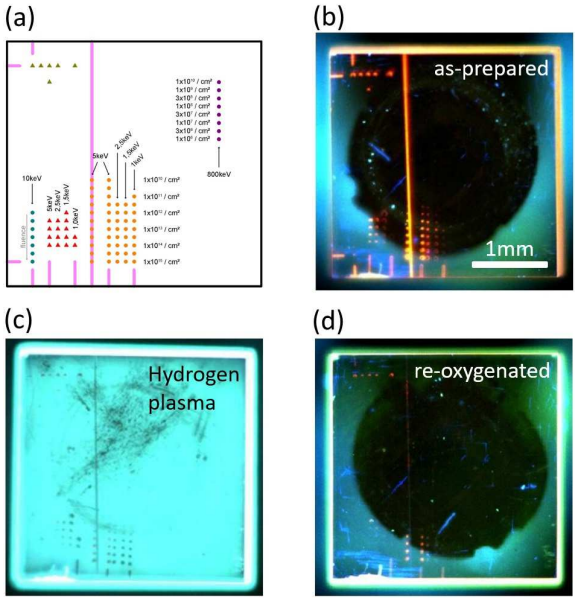

Figure 8. Hydrogen diffusion and passivation of NV centres. (a) Scheme of a 3×3 mm^2 (100) electronic grade CVD diamond implanted with nitrogen ions of different energies (1 – 800 keV) and fluences. (b) Wide field fluorescence image recorded with a "diamond view" setup (the UV source enables above-bandgap excitation). After implantation, the sample was annealed at 800°C (2 hours in vacuum) and cleaned in a boiling acid bath (4 hours in a mixture of nitric, sulphuric and perchloric acids). (c) Image taken after hydrogenation of the surface in a CVD reactor under hydrogen plasma for 30 minutes at low temperature and low power (500°C, 1000W). (d) Image taken after re-oxygenation of the diamond surface by ozonation using an excimer UV lamp.

More specifically, it was reported by Stacey et al. [79] that hydrogen can diffuse over several tens of micrometers at 800°C with a diffusion coefficient as high as 0.6×10^{-8} cm^2/s. This was obtained by applying hydrogen plasma (at different temperatures and times) to an electronic grade diamond sample and measuring the fluorescence of NV centres as a function of the depth to deduce the diffusion length. The disappearance of the NV signal was accounted for their passivation and the building of NVH complexes which are not optically active. Deuterium diffusion was also previously reported [80,81] and estimated in boron doped diamonds to study the passivation of boron acceptors. Much lower diffusion coefficients of about 5×10^{-14} cm^2/s were reported at 550°C, which could be increased up to 1.6×10^{-11} cm^2/s under bias-assisted deuteration applying 80 V [81b].

We have also studied the passivation of NV centres using implanted nitrogen into a (100) electronic grade single crystal sample at different ion energies and fluences, as seen in Figure 8a. After an 800°C annealing to form NV centres, the sample was cleaned in a boiling acid mixture to prepare an O-termination of the surface. PL images of the whole sample were acquired with a DiamondView™ setup that uses UV light (200 nm – 230 nm) to excite the luminescence. The 25 µm diameter NV ensemble spots are clearly visible. The detection limit of the setup is estimated to be 1.5×10^{10} NV cm^{-2}, from the least visible NV spot. Figure 8b shows the image of the sample as prepared, where the NV patterning

can be easily recognised. The sample has then been hydrogenated in a CVD reactor for 30 minutes under a hydrogen plasma, at a low temperature of 500°C and low power (1000W) to avoid any surface etching. The PL image after the hydrogen plasma can be seen in Figure 8c, using the same measurement conditions. Surprisingly, an intense blue fluorescence is observed, however not at the position where the NV centres are present, which appear as dark spots quenching this blue fluorescence. The origin of this fluorescence is not yet understood but near surface strain induced by the polishing might be involved. The diamond surface was then re-oxygenated, placing the sample twice for 3 minutes in a plasma cleaner under oxygen and then using an ozonation treatment (30 minutes under O_2 using a UV excimere lamp at 172 nm) which are routinely used to ensure a good O-termination. The result is shown in Figure 8d. Compared to Figure 8b, the NV fluorescence is strongly reduced, although the surface termination and measurement parameters are the same. A rough estimation indicates that the intensity is reduced by one order of magnitude, indicating that an average of about 90% of the NVs were passivated, possibly forming very stable NVH defects. Note that the depth of the NV centres here is of up to 25 nm only, which is orders of magnitude less than the NV passivation due to H diffusion reported for distances of several tens of µm in [79]. The question of hydrogen diffusion in diamond is still open and we discuss it further in the next section in which overgrowth experiments were conducted. This is an important issue to consider for the engineering of defects in diamond, especially with the presence of impurity dopants or other point defects.

3.4 Diffusion of Hydrogen – CVD overgrowth

For diamond-based quantum information processing, the optical centres used as quantum bits need to be placed precisely and close to each other within the diamond lattice. This is a challenging task when the requirements for inter-distance is of about 30 to 50 nm. It was however shown that high-resolution ion implantation of NV centres below 20 nm is possible [35], as revealed by sub-diffraction STED microscopy (see section 4.4). Nevertheless, it implies the use of low ion energy of a few keV (to minimise ion straggling [69]) which leads to the creation of very shallow centres, that are sensitive to surface defects. One possible method consists in overgrowing the implanted centres by CVD in order to bury them and improve their properties, as already demonstrated for the enhancement of the spin coherence time [82] and the charge state stabilisation [73]. However, due to the use of CVD overgrowth, hydrogen diffusion may take place and passivate the shallow implanted optical centres. We have conducted several overgrowth experiments using three types of diamond samples (one “optical grade” and one “electronic grade” from element 6, and one as-grown CVD layer) which were previously implanted with NV centres at different shallow depths (between 1 keV and 5 keV). Typically, a few µm of diamond were overgrown in the standard growth conditions for high-purity material (850°C, 3000 W, 200 mbar, 4% CH_4). Figure 9a and 9b present the result of the overgrowth on the optical grade sample which contains NV centres within the whole diamond volume. No passivation of NV centres was observed after the overgrowth at the µm depth scale: the characteristic inclined layers richer in N and NV centres are still present after the overgrowth. This is different from the results of reference [79] for which NV passivation is observed several tens of µm below the surface. However, at the nm depth scale (Figure 9c), the implanted NV centres have been passivated in different amounts, depending on the NV density, as resumed in Figure 9e (violet triangles, sample 1). This figure plots the ratio of NV centres measured after overgrowth with respect to the initial density. For the fluence of 3×10^{12} and 1×10^{13} cm^{-2}, 83% and 59% respectively of the NV centres have “disappeared”. For the higher fluences, we observe an apparent increase in the NV density which we attribute to an improvement of the diamond quality during the overgrowth. Figure 9d shows confocal scans of patterns of NV centres implanted at different depths. The surprising effect here is that the shallower NV centres survived the overgrowth whereas most of the deepest ones have disappeared.

For the same NV density, the passivation generally increases with the depth, for the 3 overgrowths. This is to be understood taking into account the N density. As seen in Figure 6b, the creation yield NV/N strongly depends on the energy within the energy range used here. Therefore, a 5-keV NV-centre is surrounded by about 25 to 100 nitrogen, whereas the creation of one 1-keV NV-centre required the implantation of at least 10 times more nitrogen. We believe that this excess in nitrogen (and unhealed implantation defects) provides more traps for the diffusing hydrogen, therefore effectively reducing

the passivation of the NV centres when the implantation energy is decreased. Furthermore, a fluence dependence is also observed in figure 9e for the two other samples too. A slight etching of the initial diamond surface during the overgrowth cannot be excluded and might be the reason for the highest loss of NV centres in the fluence range 10^{12} – 10^{13} cm^{-2}. Nevertheless, these results suggest that hydrogen diffusion takes place, at least on several tens of nm in our conditions, and that it needs to be taken into account, especially for CVD layers.

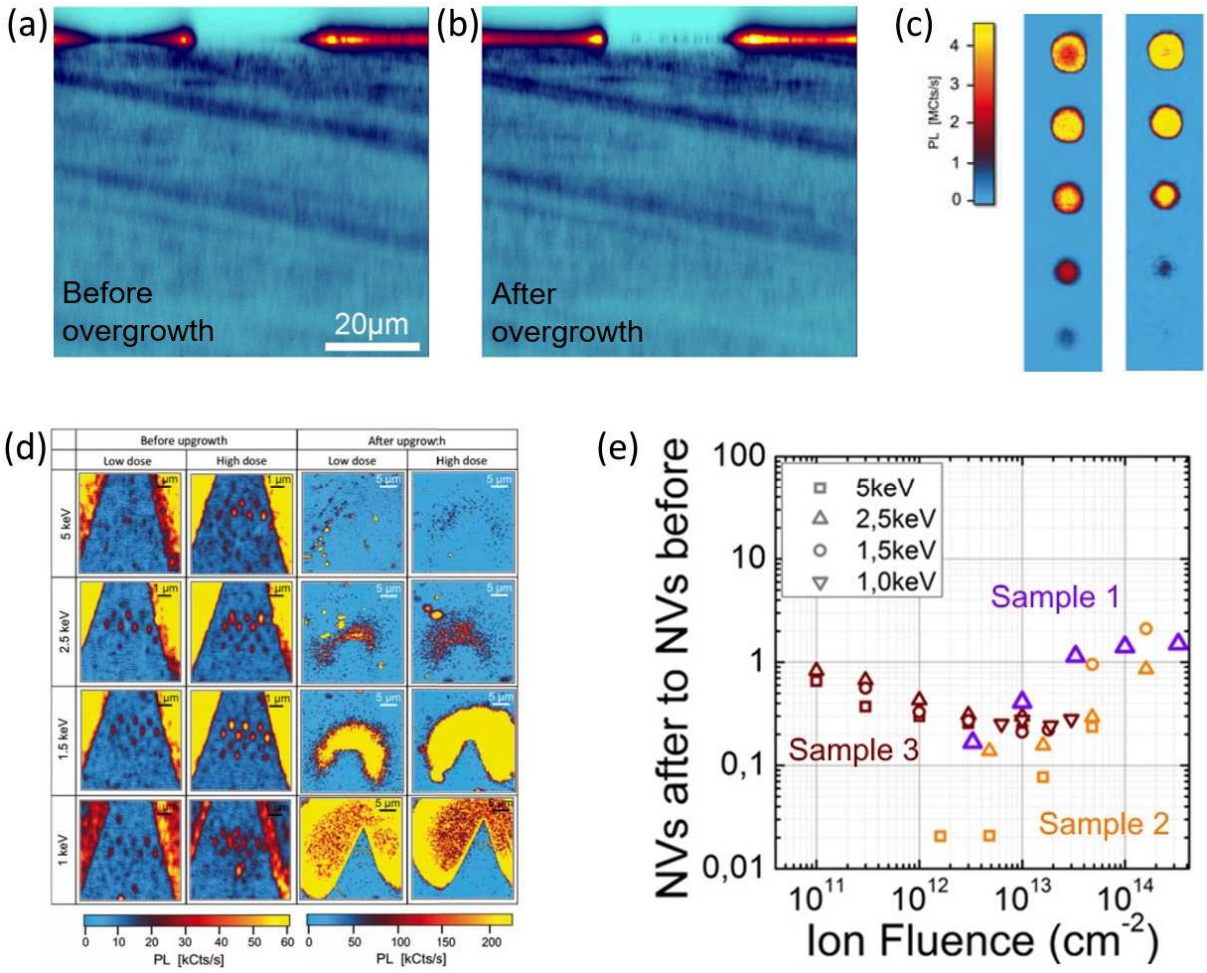

Figure 9. Hydrogen diffusion and NV passivation during CVD growth. (a) Depth confocal fluorescence scan (XZ) of an "optical grade" CVD diamond. The inclined horizontal lines (typical for CVD growth richer in nitrogen and NV centres) are used as reference for depth passivation. The laser excitation is 532 nm and the detection window 660 – 735 nm. (b) Same sample after overgrowth. No passivation can be observed at the µm scale although shallow NV centres have been passivated. (c) The sample was implanted on surface with shallow NV centres (N^+ at 2,5 keV). The left line shows surface scans of the NV centres spots (25 µm diameter) before overgrowth. The right line shows the implantation spots after CVD overgrowth at 850°C, xxx W during xxx minutes. (d) Confocal fluorescence scans showing the passivation of shallow single NV centres and ensembles, as a function of their depth, during a CVD overgrowth process. (e) Gain/loss of NV centres (ratio between NVs after and NVs before) as a function of the fluence and the implantation energy for three overgrowth processes.

An annealing at 1600°C for 2 hours has been done and no NV centre could be found after they have been passivated. This confirms that NVH centres are very stable and cannot be easily dissociated. It would be of interest to check what happens for other kinds of optical centres such as the SiV, SnV, ST1 or L1 centres.

4 Quality control of implanted colour centres and diamond substrates

The applications of optical centres in diamond for quantum information processing or quantum sensing push the requirements on the material quality and on the reproducible and nanometer placement of these centres to their limits. The multi-purpose sensing capabilities of the NV centre (magnetic and electric fields, chemical potential, temperature, stress) can be used to sense the material quality and homogeneity. Therefore, in our screening study, we always implant nitrogen as a reference or witness of the diamond matrix hosting the other defects that we create by implantation. In this section, we discuss four methods that we propose to apply complementarily to improve reproducibility in the creation of the different optical centres:

- Time trace analysis of the fluorescence (or single-shot charge-state readout) of single NV (or other) centres in order to sense the electrical environment through the stability or the blinking dynamics.
- NV-based optically detected magnetic resonance (ODMR) to sense the magnetic and electric environment as well, through the measurement of the coherence time T_2 or T_2^* of the electron spin of single NV^- centres.
- Cross-polarisation analysis in transmission in order to visualise the residual stress within the diamond sample, as well as extended defects such as dislocations.
- Stimulated Emission Depletion (STED) microscopy: in the context of building scalable arrays of qubits based on NV, ST1 or other centres, the control of their relative distances can be done optically by sub-diffraction imaging such as STED [83]. However, not all centres can be imaged with this technique because it requires a large shift between the emission and absorption bands. In this section, we show how STED can also successfully be applied to the recently discovered and promising ST1 centres [2,3] and we discuss its potential application to GR1 centres (neutral vacancies) which would be of high interest for the defect engineering in diamond.

4.1 Charge state and fluorescence stability – time trace analysis

The fluorescence and charge state stability of defect centres is an important issue for their reliable use as sensors, qubits or single-photon sources. Although they can be seen as artificial atoms in the solid-state, the close environment of implanted centres may vary from one to the other due to many process steps, to diamond quality, homogeneity and impurity level, or due to the surface state and/or preparation. In diamond, no general chemical potential can be defined as in standard semi-conductors [84], thus the optical centres can be found in different charge states at different locations within a diamond sample. This is illustrated in Figure 10a which shows three implanted L1 centres (separated by only a few µm) in an electronic grade CVD (100) diamond sample. The confocal fluorescence scans are all taken under the same excitation conditions (excitation laser 532 nm, 500 µW, scan speed 5 µm/s) and it can be seen that the three L1 centres show drastically different stability and blinking properties. The charge states of the L1 are not yet known, however the blinking is likely due to surface states or neighbouring donator or acceptor states. The fluorescence stability and/or blinking dynamics can be followed by recording the time-trace of the fluorescence as in Figure 10b. A stable L1 centre would be useful as a single photon source whereas a fast-blinking L1 would be suitable for stochastic sub-diffraction imaging such as stochastic optical reconstruction microscopy (STORM) [85] or photoactivated localisation microscopy (PALM) [86]. The ionising and charging rates can be deduced and plotted as a function of the laser power (Figure 10c) or excitation wavelength. They can therefore be used as a footprint of the centre´s environment and we propose to use this technique for quality control of optical centres.

Many efforts were done to stabilise [87,88] and/or tune and control the charge state of colour centres, especially with the NV centre: chemically [89-92], optically [93], electrically [17,18,94,95]. It was shown by single-shot charge-state readout that the NV centres charge state is constantly “jumping” between NV^- and NV^0 under light excitation due to photo-induced ionisation and recharging [96]. These rates depend on the laser excitation power and wavelength. This is illustrated in Figures 10d and 10e for a single NV centre into an electronic grade CVD diamond. In addition, the presence of donors or acceptors is expected to strongly modify the charge state dynamics. This is shown for single NV centres

in the case of an N-rich HPHT diamond (Figures 10f and 10h) and of a B-rich CVD-grown diamond (Figures 10g and 10i). The NV^- state is stabilised by the presence of the nitrogen-rich surrounding, which acts as a deep donator (1.7 eV) that can be ionised by the laser excitation and provide free electrons. As well, the presence of boron (0.37 deep acceptor niveau) induces the blinking of the NV centre. A model was proposed in [96] in good agreement with the two-photon processes observed in the quadratic variation of the ionisation and recharging rates as a function of the excitation power.

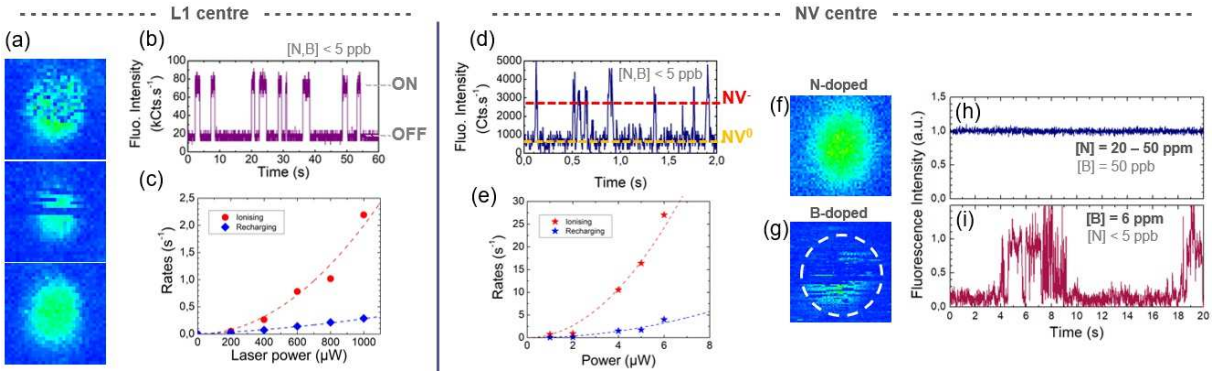

Figure 10. Time trace analysis for charge state and fluorescence stability. (a) Confocal fluorescence scans (1×1 µm²) of three different L1 centres implanted into an electronic grade CVD diamond (laser excitation at 532 nm and detection within 575 – 630 nm). The centres are separated by only a few µm but show different stability/blinking under the same excitation conditions. (b) Time trace of one of the moderately blinking L1 centres at a laser power of 800 µW. (c) Power dependence of the ionising and recharging rates of the moderately blinking L1 centre at 594 nm excitation. (d) Time trace of a single NV centre in an electronic grade CVD diamond enabling charge-state single-shot readout (excitation 594 nm, 5 µW, detection 660 – 735 nm). With the 594 nm laser used here (5 µW), fluorescence is observed only when the NV centres is negatively charged. The charge state jumps are photo-induced by the laser [96]. (e) Power dependence of the ionising and recharging rates of the single NV centre. (f) Fluorescence image of a single native NV centre within a HPHT sample with [N] of 20 to 50 ppm. (g) Fluorescence image of a single NV centre implanted into a boron-doped CVD layer with [B] about 1×10^{18} cm^{-3} (6 ppm). For both scans, the laser excitation is 594 nm and the detection window 660 nm – 735 nm. (h) and (i) Time trace analysis of the two centres with P = 800 µW for the centre in (f) and P = 230 µW for the centre in (g). The charge state changes between NV^- and NV^0 are due to the boron (acceptor) doping.

4.2 Spin coherence time – NV-based ODMR

The spin properties of the NV centres at room temperature permit to use the NV centre as a nanoscale and sensitive "multi-task" quantum sensor. Within the screening method presented here, we always implant NV centres as well, to give insights into the diamond material into which we produce other kinds of optical centres. The NVs are well suited to measure electronic and magnetic impurities, which reveal their presence on the coherence time of the NV^- centre. For example, it was shown in [97] that the broadening of the ESR lines of single implanted NVs is depending on the depth due to the presence of surface paramagnetic impurities. The spin coherence properties and the charge state stability of such shallow centres can be improved by diamond overgrowth [73,82]. Isotopically ^{12}C enriched samples with [^{13}C] of about 0,3% (instead of 1.1% natural abundancy) led to long T_2 times of up to 1.8 ms at room temperature [98]. Furthermore, the radiation defects can be probed by NV-ODMR. The etching of a thin superficial diamond layer above the implanted NV centres revealed an improvement of the coherence time due to the removing of the vacancies induced by the ion implantation process present in this layer [71]. As well, the correlation between annealing temperature and healing of vacancies complexes along <111> (measured by electron paramagnetic resonance) was shown in [59]. Also, the study of the hyperfine couplings to the electron spin of the NV^- centre can be used to retrieve atom species which are close by, such as described in [99].

4.3 Diamond homogeneity – Cross-polarisation analysis

The observation of a transparent material in transmission, placed between two polarisers having their axis perpendicular to each other, enables the visualisation of birefringence. Applied to an isotrope

material such as diamond, this method enables a direct view of the stress within the diamond substrate as shown in Figure 11a. The strain induces a change in the refractive index of diamond and the appearance of birefringence. Even though a quantitative analysis is hardly achievable [100], this method reveals dislocations (Figure 11b) and therefore dislocation-free regions can be easily pre-selected. The homogeneity of the diamond sample (in terms of these defects) is easily made visible with this non-invasive and fast method. Stress is for example responsible for shifting the ZPL emission of most of the optical centres. It is therefore important to know the stress and sample homogeneity.
As an example, we present in Figure 11c the results of strong variations in the creation of NV centres by nitrogen implantation. These variations cannot be explained by ion beam current fluctuations during the implantation process because the implantation pattern was scanned a hundred times (with the ion beam focused down to 1 µm) to reach the total fluence per point (and not one point after the other with the full fluence implanted in one shot). Interestingly, we found these spatial variations in the creation efficiency of NV centre within a CVD diamond layer presenting the birefringence patterns observed in Figure 11b and having the same orientation and size. We believe that the stress likely plays a role during the annealing step and influences the diffusion of vacancies. This may enable the fabrication of single centers with improved creation yields and further experiments are needed to clarify this. Cross-polarisation analysis is a very fast and non-invasive method which can be used to preselect the suitable areas of a diamond sample for quantum application using optical centres.

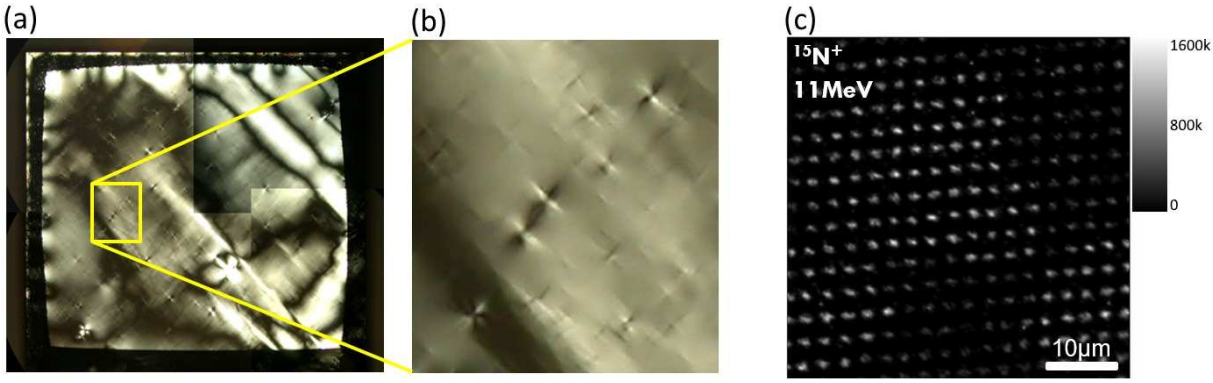

Figure 11. Diamond inhomogeneities. (a) Transmission optical image with crossed polarisers of a thin CVD diamond layer grown on a HPHT substrate (3×3 mm²). The observed birefringence reveals the inhomogeneity of stress and the presence of defects within the diamond layer. (b) The inset shows typical "flower" patterns due to dislocations or bunches of dislocations induced at the CVD overgrowth. (c) Confocal fluorescence scan of an array of NV centres implanted in diamond with a beam of 11 MeV N^+ ions focused down to 1 µm, corresponding to an implantation depth of 5 µm. This array was produced by scanning the same pattern a hundred times in order to ensure a homogeneous fluence per point and to average out the short-time scale fluctuations of the ion beam flux. Similar behaviours are observed for an implantation energy of 2 MeV corresponding to a 1 µm depth (not shown).

4.4 High-resolution implantation – STED microscopy

In standard confocal fluorescence imaging, the separation power Δr of the setup is given by the Abbe´s criteria

$$\Delta r \approx \frac{\lambda}{2\,NA}$$

where NA is the numerical aperture of the objective. The point-spread function is an ellipsoid of dimensions of about 300 nm in transverse and 1 µm in longitudinal directions. Two point-like emitters located within this ellipsoid can therefore not be optically resolved. With the introduction of new nanoscopy methods such as STED [83], STORM [85] or PALM [86], it became possible to beat the diffraction limit. An improvement of more than one order of magnitude was demonstrated in the case of STED imaging of NV centres in diamond [35,101]. This was possible thanks to the extreme robustness and optical stability of this system which is able to sustain high laser intensities without bleaching. Indeed, the STED resolution is not unlimited and is given by

$$\Delta r_{STED} \propto \frac{\lambda_{STED}}{\sqrt{I_{STED}/I_{sat}}}$$

where I_{STED} is the intensity of the STED depletion beam and I_{sat} is the saturation intensity of the optical centre. Figure 12a shows an implanted array of shallow NV centres imaged by confocal microscopy with $\Delta r_{confocal} \approx 250$ nm and Figure 12b shows the same array imaged by STED microscopy with $\Delta r_{STED} \approx 10$ nm.

The fabrication of scalable structures based on optical centres in diamond is highly challenging especially because the deterministic fabrication of NV, ST1 or other centres is not yet achieved. However, the deterministic implantation of single ions was already demonstrated using a modified Paul trap [38] and bunches of ions can be detected on-the-fly using image charge detection [39l] which could become soon a versatile deterministic ion implantation method. On the other hand, the spatial placement within less than 20 nm was already demonstrated with NV centres [35] and is very promising to create QIP structures. To date, only two optical centres in diamond, the NV and the ST1, were found to show ODMR at room temperature [2,3].

Here, we show that STED can also be applied efficiently to the ST1 centres. Moreover, the optical properties of the ST1 enable to use the same wavelengths for excitation and depletion as for the NV centre. The fluorescence spectra of the NV and ST1 centres are compared in Figure 12c, together with the one of the GR1 centre (neutral vacancy). Figure 12d is a confocal scan of randomly distributed L1 and ST1 centres. STED was driven on one of the ST1 centres as shown in Figure 12e, which plot together a confocal and a STED scan. The dependence of the lateral resolution as a function of the STED intensity is plot in Figure 12f, together for the NV and the ST1 centres. This shows that STED imaging of the most promising centres for QIP is possible, moreover using the same excitation and depletion lasers. In the purpose of defect engineering, it would be of interest to image by STED the single vacancies in order to improve and refine the understanding of the discussion found in the first part of this work. This would imply first to image single vacancies by confocal microscopy which has not yet been shown.

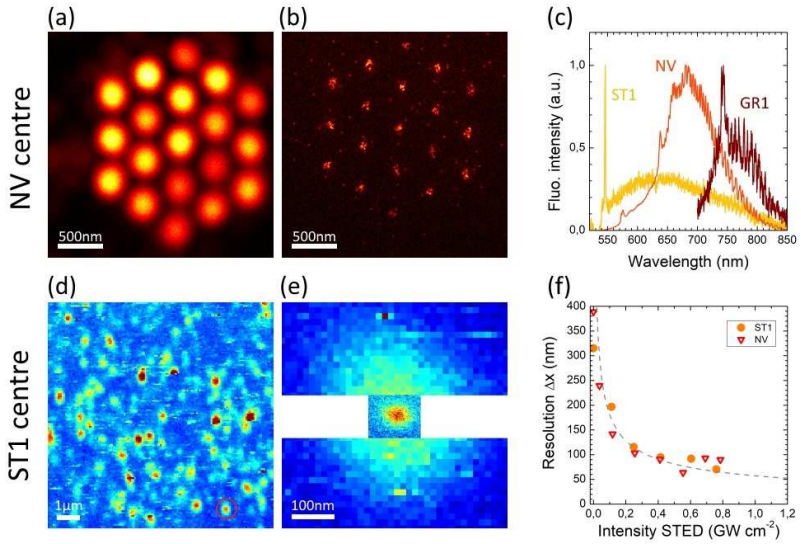

Figure 12. STED microscopy of NV and ST1 centres. (a) Confocal scan of an array of NV centres created by nitrogen implantation through a pierced AFM tip. The optical resolution of the image is limited by diffraction. (b) STED image of the same area, with an optical STED resolution of 10 nm. (c) Fluorescence spectra of the ST1, the NV and the GR1 centres. (d) Confocal scan of a diamond sample containing L1 and ST1 centres. (e) Combination of a confocal and of a STED image of a single ST1 centre (shown by the red circle in Figure 12b). (f) Lateral resolution as a function of the STED beam intensity for the NV and the ST1 centres. The saturation intensity of NVs is given in [101] to be 6.6 MW cm^{-2} and it was found to be similar for the ST1 centre.

5 Investigation of colour centres in diamond

This section is dedicated to the preliminary results of the screening study, concerning more particularly the elements O, F, Mg, Ca and P, which all were found to produce optically active defects. The nuclear-spin-free elements ^{16}O, ^{24}Mg and ^{40}Ca were particularly of interest in the context of the search for the ST1 centre.

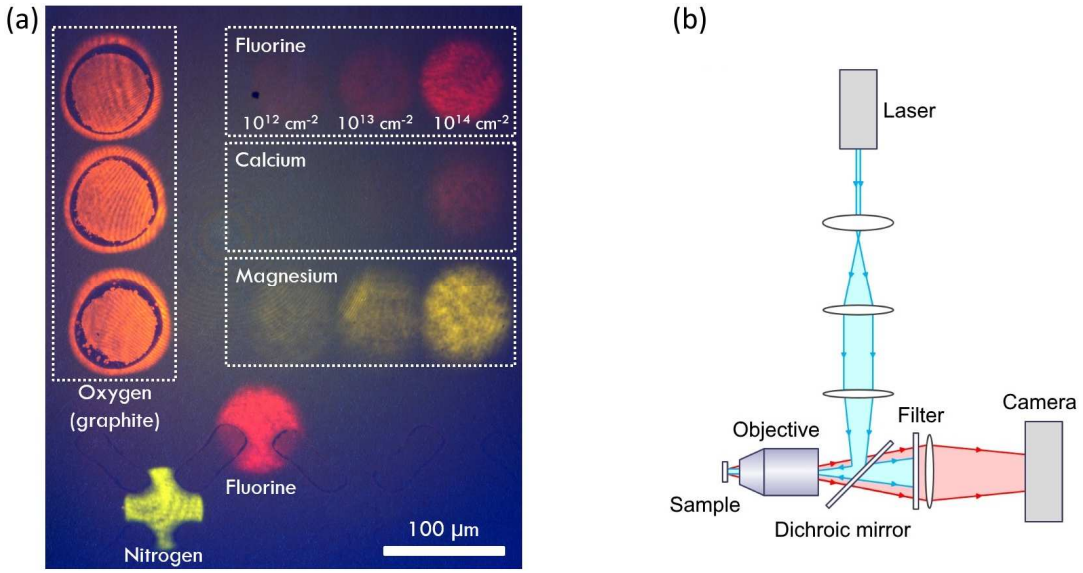

Figure 13. (a) Wide field fluorescence image of a "screened" diamond sample implanted with N, O, F, Mg and Ca and annealed up to 1600°C. The objective used is an Olympus ×20 with NA = 0.5. A f = 30 cm lens was used to form the image on the camera sensor, corresponding to a magnification of 38. The excitation wavelength is here 488 nm (35 mW at the entrance of the objective) and the fluorescence is filtered with a dichroic mirror (cutoff wavelength of 550 nm) and a Notch filter (488 nm). An area of about 0.2 mm² of the diamond is illuminated. The image is taken with a commercial camera Sony α 77 II with an ISO value of 200 and an integration time of 20 s. (b) Scheme of the home-built wide field microscope dedicated to the characterisation of the screened sample. The setup is versatile and enables to change the light source, the objective and the magnification fast and easily.

As described in section 1, our method consists in implanting different chemical elements within a same sample and using, at first, wide-field techniques for high throughput, and then confocal fluorescence microscopy (or even sub-diffraction microscopy) for a deeper targeted study. In this purpose, we have built a home-made and versatile wide-field fluorescence microscope, as schemed in Figure 12b. The laser source, the objective and the imaging lens can be easily changed and adapted to the sample and fluorescent centres in order to obtain fluorescence images in one shot. The sample used here is a single crystal (100) CVD "electronic grade" from element 6 presented in 1. Due to the lower sensitivity of the wide-field setup (compared to scanning confocal fluorescence microscopy) high implantation fluences are used to ensure strong fluorescence signals (10^{12} cm^{-2}, 10^{13} cm^{-2} and 10^{14} cm^{-2}). Nitrogen was also implanted as a reference (30 keV, 10^{14} cm^{-2}). Three graphite spots were produced for orientation using ^{16}O ions at very high fluence of 10^{16} cm^{-2}. The implantation through an aperture placed a few mm away from the diamond surface (Figure 1b) induces a fluence gradient around the spots, allowing to study the fluorescent centres at the single centre level in case they are bright enough. The sample was annealed for 4 hours at 1600°C in vacuum. The surface was cleaned in an oxygen plasma chamber, which removed most of the graphite from the oxygen spots. A typical wide-field image of this screened diamond with the elements O, F, Mg and Ca is shown in Figure 12a, in real colours. It was recorded in one shot (20 seconds acquisition time) with a commercial photo camera. The wide field image shows that each implanted element produces fluorescence, and give rough but fast insights about their brightness and spectral emission before more precise measurements methods are employed.

5.1 Oxygen

One of the aims of the screening method is to try to reproduce defects of still unknown nature. It was recently shown that ST1 and L1 centres were created together, within the same sample and ion implantation run. The ST1 centres show ODMR at room temperature but no hyperfine coupling was found in their ODMR spectra, indicating that the constituent atom likely possess no nuclear spin. One of the candidates is ^{16}O, supported by the fact that the two creations methods of ST1 involved oxygen: (i) RIE etching [2] and ion implantation using a cathode with B, C, N, and O in it [3]. We have recently implanted oxygen at low fluence and annealed the sample at 800°C in order to find single centres. No L1 or ST1 could be found. Here we have used a much higher ion fluence with a gradient up to $1x10^{16}$ cm^{-2} and an annealing temperature of 1600°C. Indeed, we observe the creation of O-related colour centres having an intense orange fluorescence (Figure 13a) with a ZPL likely at 584.5 nm and a broad phonon sideband of about 120 nm (Figure 14a). The same spectra are found both in the corona and in the centre (after removal of the graphite of the O-spots). This centre was already reported in [102] in the case O^+ implantation and after annealing above 1600°C only. Another line at 598.4 nm was also attributed to the O implantation but we do not observe it here. This high-density high-temperature treatment of oxygen can be put in parallel with nitrogen. At low fluence and low temperature annealing (800°C), mostly NV centres are produced. However, at higher fluences and higher temperatures, it becomes more likely to form H3 centres (ZPL at 503 nm) due to diffusion of nitrogen (see section 3.2). In order to "spy on" the oxygen centres, we have also implanted nitrogen at high fluence to check whether H3 centres also form. The green-yellow fluorescence seen in Figure 12a reveals the presence of H3 centres in majority, which is confirmed by the spectrum shown in Figure 13b. These O-related centres may be due to O complexes. However, neither the optical spectra of the ST1 (ZPL at 546 nm and broad phonon sideband) nor of the L1 (sharp and strong ZPL around 580 nm) resemble the O-centre shown here.

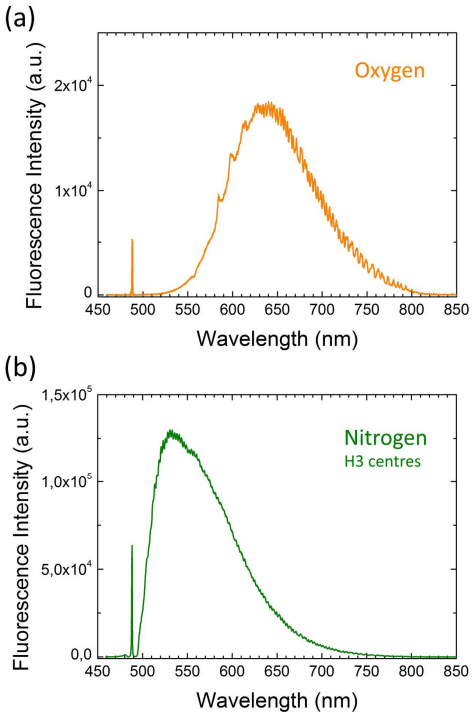

Figure 14. (a) Fluorescence spectrum taken in the corona of the graphite spot produced by oxygen implantation using a confocal microscope. The excitation is 488 nm. The spectrum is background corrected using a reference spectrum taken away from the implantation. As also seen in Figure 4, the corona presents a radial fluence gradient of oxygen and the O-related fluorescence is expected to be found in a fluence range 10^{13} – 10^{14} cm^{-2}. (b) By analogy to the nitrogen implantation, the 10^{14} cm^{-2} nitrogen spot shows H3 fluorescence, confirming the high temperature treatment at 1600°C.

5.2 Calcium

The most naturally occurring isotope of calcium, ^{40}Ca with 97% abundance, is free of nuclear spin. The orange fluorescence observed in Figure 13a from the Ca spot might be a candidate to correspond to the ST1 fluorescence. However, the brightness of the Ca-related fluorescence is weak and no single centres could be found. The fluorescence spectrum taken from the spot of highest fluence is shown in Figure 15b. It possesses a ZPL at 557 nm and a broad phonon sideband which do not correspond to the ST1 centre.

5.3 Fluorine

The red fluorescence observed in Figure 13a from the F spot is about 30 times brighter than the Ca-related emission. The fluorescence spectrum taken from the spot of highest fluence is shown in Figure 15a. A broad emission peak centered at 680 nm is observed without any visible ZPL.

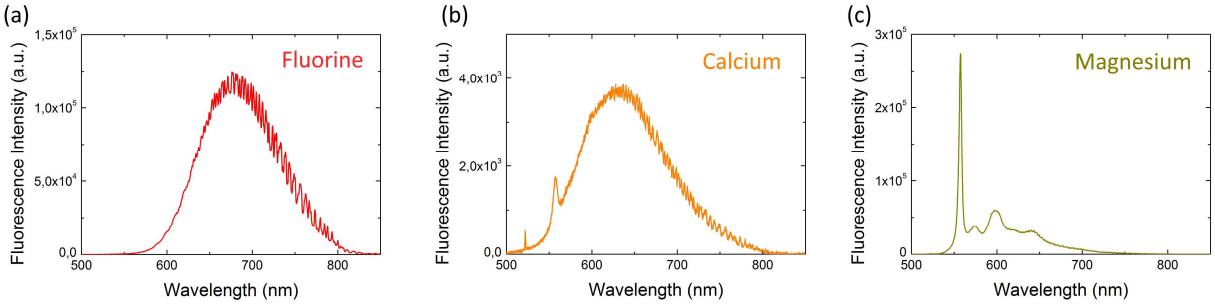

Figure 15. Fluorescence spectra of (a) the F-related centres, (b) the Ca-related centres and (c) the Mg-related centres, using a 488 nm excitation. The same experimental conditions are used for all the measurements.

5.4 Magnesium

The isotope ^{24}Mg (abundancy of 79%), free of nuclear spin, is also a potential candidate to be involved in the ST1 defect. The fluorescence spectrum of an ensemble of Mg-related centres is shown in Figure 15c. It possesses a sharp and intense ZPL at 557 nm and the vibronic sideband presents features at 66 meV and 154 meV. Although some single ST1 centres were reported with ZPL emission above 550 nm, the sideband are rather different. The Mg fluorescence is strong and a weak peak was already observed directly after implantation without annealing. Figure 16a is a confocal fluorescence close view (15×15 µm²) taken at the edge of the Mg-implanted area with fluence of 1×10^{13} cm^{-2}. Single emission spots appear, forming a halo around the main implantation area. We then further check whether they are single Mg-related centres. A fluorescence spectrum of one of these spots is plotted in Figure 16b which confirms that they possess the same fluorescence as the ensemble measurement of Figure 15c, thus confirming the involvemement of Mg. The single quantum emitter behavior of one of these spots is proved by the antibunching observed in the photon autocorrelation function $g^{(2)}(\tau)$ plotted in figure 16d. The curve is fitted with a three-exponential function. The lifetime of the excited state can be deduced from the fit and we obtain about 2,3 ns, shorter than the 9 ns of the ST1 centre. The bunching behaviour indicates the presence of two shelving states with time constants of about 150 ns and 2,4 µs. A typical saturation curve for a single Mg centre is schown in figure 16c. It has been fitted as follows

$$I = I_\infty \frac{1}{1 + {P_s}/{P}} + bP$$

where I_∞ is the saturation count rate, P_s is the saturation power and and b the linear contribution of the background fluorescence. We obtain $I_\infty = 3.3\times10^5$ counts s^{-1}, a saturation power of 5.1 mW and $b \approx 3.82\times10^4$ counts s^{-1} mW^{-1}.

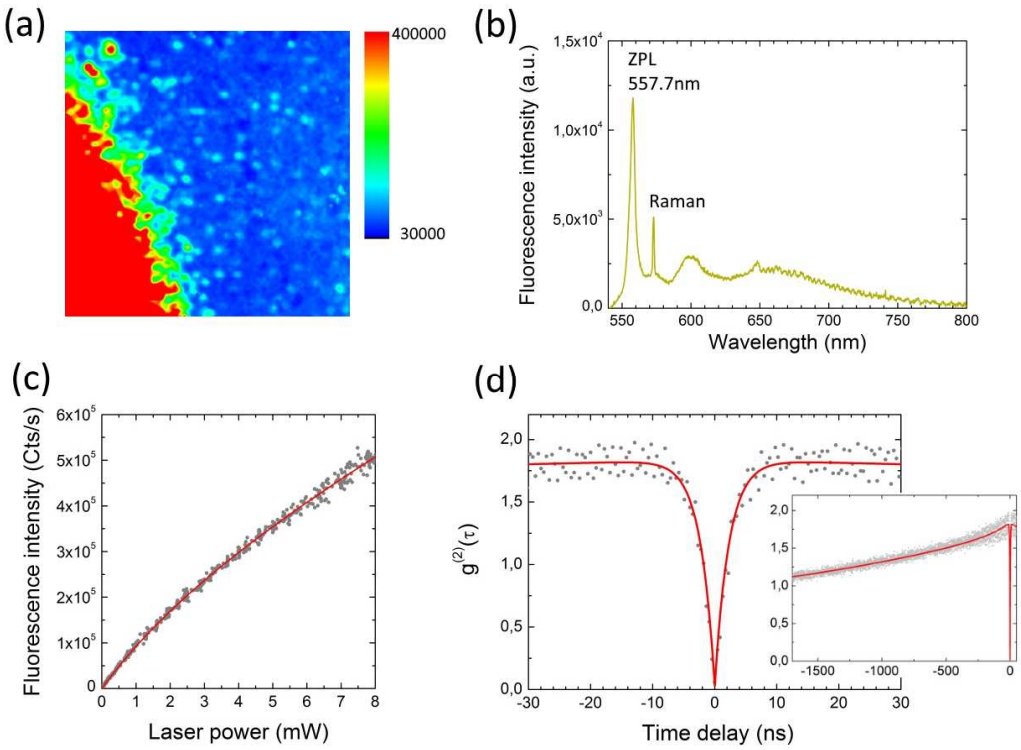

Figure 16. Single Mg-related centres. (a) Confocal fluorescence scan recorded at the border of a Mg implantation spot (energy of 50 keV, fluence 10^{13} cm^{-2}) with an excitation wavelength of 532 nm. (b) Fluorescence spectrum of a single Mg-related centre (excitation power 4 mW, 125s integration time). (c) Saturation curve of a single Mg centre. (d) Photon autocorrelation function $g^{(2)}(\tau)$ measured at a laser power of 1.44 mW. The curve is background corrected and normalised. The dip going to zero at zero time delay proves the single quantum emitter behavior of the defect. The exponential fit gives a lifetime of 2,4 ns for the excited state. The inset shows the $g^{(2)}(\tau)$ function for longer times.

With the measurement of single Mg centres, it becomes possible to estimate the creation yield of the Mg centres, with respect to the number of implanted Mg atoms. Taking an average fluorescence intensity in the implantation spot of fluence 10^{13} cm^{-2}, we obtain a creation yield of about 12%. Note that this corresponds to an annealing done at 1600°C for 4 hours. Further study is required to follow the temperature evolution of the Mg-related fluorescence.

The optical properties of these Mg-related centres measured in an intrinsic region of the diamond sample indicate that it is a different defect than the ST1 centre. Note that several Mg-related centres were spectrally studied and the ZPL emission was found in the range 557 – 562 nm. Finally, we have searched for ODMR within the microwave frequency range 0.5 to 4 GHz with 1 MHz resolution and did not find any resonance.

5.5 Phosphorous

Phosphorous is one of the possible donators in diamond, however with a deep level placed 1.7 eV below the conduction band. This means that at room-temperature, no free carriers can be found in the conduction band. However, the charge state of optical centres can be influenced in a compensation way by the presence of donators in their vicinity [87,88]. Ion implantation and annealing are generally considered to be a less efficient method to produce substitutional P compared to CVD growth due to the presence of radiation defects acting as compensation centres. Note that up to 70% of substitutional phosphorous was reported by implantation and annealing, as measured by emission channeling technique [103]. Reference J. Barjon

Here, we found that the implantation of P followed by high temperature annealing (4 hours at 1600°C) in vacuum leads to the formation of luminescent centres with a very low creation yield. This can be seen in Figure 17a, where the border between the P-implanted area and the unimplanted area

(covered with an aluminum foil) are imaged with confocal microscopy. Single spots with an average density of about 1.5 μm^{-2} are visible. The P implantation conditions were determined to obtain P atoms at an average depth of 50 nm with a total fluence of $1.6x10^{13}$ cm^{-2}. This indicates a creation yield of about 10^{-5} with respect to the number of implanted phosphorous atoms. Moreover, two kinds of centres are observed as plotted in Figures 17b and 17c, with ZPL at 557 nm or with a doublet of lines at 579.4 nm and 597.2 nm. These centres were visible only after the annealing and might involve vacancies. It is not yet clear what these likely P-related centres can be. It was however theoretically predicted that PV^- centres do not possess an optical transition and act as compensation centres of n-type doping [104]. The high temperature and long annealing time used, together with the relatively high phosphorous density of about 3×10^{18} cm^{-3} might imply more complex defects than PV, by analogy with the H3/NV ratio studied in section 3.2.

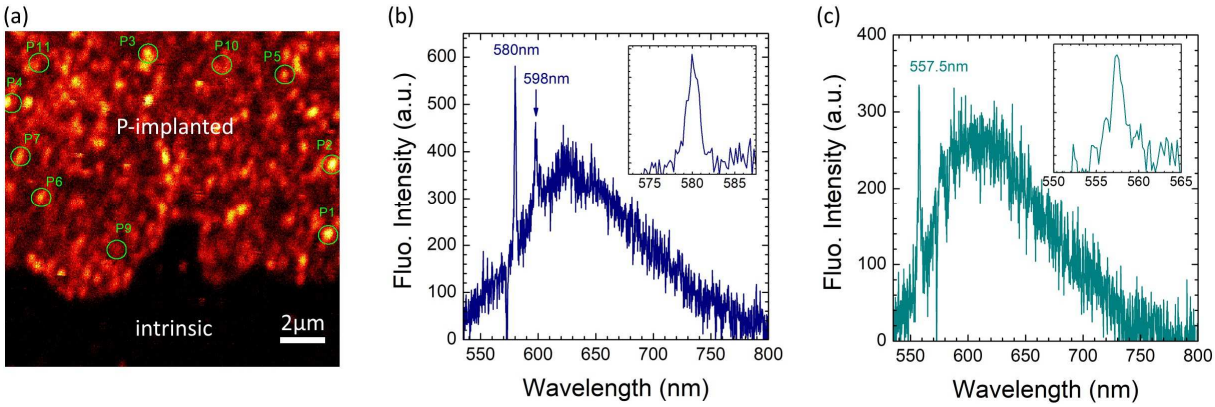

Figure 17. (a) Confocal scan at the border of a phosphorous-implanted region of the diamond sample. (b) Fluorescence spectra (background-corrected) of single fluorescent spots of first type in the phosphorous implanted area. (c) Fluorescence spectrum of the centres of second type.

Summary

In this paper, we have presented a high throughput screening method for the search, the reproducible creation and the identification of single defects in diamond. We used a versatile ion accelerator to implant several chemical elements and we applied optical imaging and spectroscopy to study the defects created and their temperature evolution. Firstly, we discussed both theoretically and experimentally the distribution of carbon vacancies produced at the end of range of an implanted ion, as well as the consequences for the creation of colour centres, depending on the atom mass and nature of the defect produced. We conducted molecular dynamics simulations which showed that the primary damage is in small disordered atom regions rather than isolated point defects. This is confirmed experimentally, we further observed that the relative amount of single vacancies (GR1) which are produced decreases with the ion mass, preferentially leading to more complex groups of vacancies.

We then discussed the formation and dissociation of different defects such as the GR1, 3H, NV and H3 under thermal annealing. More particularly, we showed using ODMR that, at 1150°C, the NV centres bond do not change orientation. At higher temperatures, we observed nitrogen diffusion through the increase of H3 fluorescence with respect to NV fluorescence and estimated the nitrogen diffusion coefficient to be 1.7×10^{-3} nm^2/s at 1600°C. We further confirmed the effect of hydrogen diffusion on the “irreversible” passivation of NV centres and quantified the NV loss in different experimental conditions. We then proposed to establish quality control of diamond material and optical centres, to improve their reproducibility. In this context, we showed that STED microscopy can be applied to the ST1 centres as efficiently as for NV centres, which is promising for the scalable creation of QIP devices based on these ODMR active centres.

Finally, the first results of the long term screening study were presented. It was found that Ca, Mg, F, O and P are inducing optically active defects in the visible. A fine study was conducted on single Mg-related centres, which were still found up to 1600°C, and which present a strong and narrow ZPL at

557 nm with a relatively weak phonon sideband at room temperature. Interestingly, single fluorescent centres were found related to the phosphorous implantation. The low creation yield and a better understanding of these centres may give insights in the compensation of phosphorous donators.
The screening will be extended to other elements, combinations of elements and to different doping and doping levels of diamond.

Acknowledgements
The authors acknowledge the support from the Deutsche Forschungsgemeinschaft (Forschergruppe 1493) as well as the European Union (DIADEMS) and the Volkswagen Stiftung.

References

[1] A. M. Zaitsev, *Optical properties of diamond*, Berlin Springer, (2001)
[2] S. Y. Lee et al., *Readout and control of a single nuclear spin with a metastable electron spin ancilla*, Nat. Nanotechnol. **8**, 487 (2013)
[3] R. John, J. Lehnert, M. Mensing, D. Spemann, S. Pezzagna and J. Meijer, *Bright optical centre in diamond with narrow, highly polarised and nearly phonon-free fluorescence at room temperature*, New J. Phys. **19**, 053008 (2017)
[4] F. Jelezko, T. Gaebel, I. Popa, A. Gruber and J. Wrachtrup, *Observation of coherent oscillations in a single electron spin*, Phys. Rev. Lett. **92**, 076401 (2004)
[5] M. W. Doherty, N. B. Manson, P. Delaney, F. Jelezko, J. Wrachtrup and L. C. L. Hollenberg, *The nitrogen-vacancy colour centre in diamond*, Phys. Rep. **528**, 1 (2013)
[6] T. D. Ladd, F. Jelezko, R. Laflamme, Y. Nakamura, C. Monroe and J. L. O'Brien, *Quantum computers*, Nature **464**, 45 (2010)
[7] F. Dolde et al., *Room-temperature entanglement between single defect spins in diamond*, Nat. Phys. **9**, 139 (2013).
[8] H. Bernien et al., *Loophole-free Bell inequality violationusing electron spins separated by 1.3 kilometres*, Nature **526**, 682 (2015)
[9] R. Alleaume, F. Treussart, G. Messin, Y. Dumeige, J.-F. Roch, A. Beveratos, R. Brouri-Tualle, J.-P. Poizat and P. Grangier, *Experimental open-air quantum key distribution with a single-photon source*, New J. Phys. **6**, 92 (2004)
[10] J. R. Maze *et al.*, *Nanoscale magnetic sensing with an individual electronic spin in diamond*, Nature **455**, 644 (2008)
[11] G. Balasubramanian *et al.*, *Nanoscale imaging magnetometry with diamond spins under ambient conditions*, Nature **455**, 648 (2008)
[12] L. Rondin, J.-P. Tetienne, T. Hingant, J.-F. Roch, P. Maletinsky and V. Jacques, *Magnetometry with nitrogen-vacancy defects in diamond*, Reports Prog. Phys. **77**, 056503 (2014)
[13] F. Dolde et al., *Nanoscale detection of a single fundamental charge in ambient conditions using the NV-center in diamond*, Phys. Rev. Lett. **112**, 097603 (2014)
[14] G. Kucsko, P. C. Maurer, N. Y. Yao, M. Kubo, H. J. Noh, P. K. Lo and M. D. Lukin, *Nanometre-scale thermometry in a living cell*, Nature **500**, 54 (2013)
[15] P. Neumann et al., *High-precision nanoscale temperature sensing using single defects in diamond*, Nano Lett. **13**, 2738 (2013)
[16] T. Plakhotnik, M. W. Doherty, J. H. Cole, R. Chapman and N. B Manson, *All-optical thermometry and thermal properties of the optically detected spin resonances of the NV^- center in nanodiamond*, Nano Lett. **14**, 4989 (2014)
[17] C. Schreyvogel, M. Wolfer, H. Kato, M. Schreck and C. E. Nebel, *Tuned NV emission by in-plane Al-Schottky junctions on hydrogen terminated diamond*, Sci. Rep. **4**, 3634 (2014)
[18] M. Pfender *et al.*, *Protecting a diamond quantum memory by charge state control*, Nano Lett. **17**, 5931 (2017)
[19] E. Bourgeois, A. Jarmola, P. Siyushev, M. Gulka, J. Hruby, F. Jelezko, D. Budker and M. Nesladek, *Photoelectric detection of electron spin resonance of nitrogen-vacancy centres in diamond*, Nat. Comm. **6**, 8577 (2015)

[20] A. Sipahigil, K. D. Jahnke, L. J. rogers, T. Teraji, J. Isoya, A. S. Zibrov, F. Jelezko and M. D. Lukin, *Indistinguishable photons from separated silicon-vacancy centers in diamond*, Phys. Rev. Lett. **113**, 113602 (2014)

[21] B. Pingault, D.D. Jarausch, C. Hepp, L. Klintberg, J. N. Becker, M. Markham, C. Becher and M. Atatüre, *Coherent control of the silicon-vacancy spin in diamond*, Nat. Comm. **8**, 15579 (2017)

[22] D. D. Sukachev, A. Sipahigil, C. T. Nguyen, M. K. Bhaskar, R. E. Evans, F. Jelezko and M. D. Lukin, *Silicon-vacancy spin qubit in diamond: a quantum memory exceeding 10 ms with single-shot state readout*, Phys. Rev. Lett. **119**, 223602 (2017)

[23] A. Sipahigil et al., *All integrated diamond nanophotonics platform for quantum-optical networks*, Science **354**, 847 (2016)

[24] T. Iwasaki, F. Ishibashi, Y. Miyamoto, Y. Doi, S. Kobayashi, T. Miyazaki, K. Tahara, K. D. Jahnke, L. J. Rogers, B. Naydenov, F. Jelezko, S. Yamasaki, S. Nagamachi, T. Inubushi, N. Mizuochi and M. Hatano, *Germanium-vacancy single color centers in diamond*, Scientific Reports **5**, 12882 (2015)

[25] S. Häußler, G. Thiering, A. Dietrich, N. Waasem, T. Teraji, J. Isoya, T. Iwasaki, M. Hatano, F. Jelezko, A. Gali and A. Kubanek, *Photoluminescence excitation spectroscopy of SiV- and GeV-color center in diamond*, New J. Phys. **19**, 063036 (2017)

[26] E. A. Ekimov, S. G. Lyapin, K. N. Boldyrev, M. V. Kondrin, R. Khmelnitskiy, V. A. Gavva, T. V. Kotereva and M. N. Popova, *Germanium-vacancy color center in isotopically enriched diamonds synthesized at high pressures*, JETP Letters **102**, 701 (2015)

[27] S. Ditalia Tchernij, T. Herzig, J. Forneris, J. Küpper, S. Pezzagna, P. Traina, E. Moreva, I. P. Degiovanni, G. Brida, N. Skukan, M. Genovese, M. Jaksic, J. Meijer and P. Olivero, *Single-photon-emitting optical centers in diamond fabricated upon Sn implantation*, ACS Photonics **4**, 2580 (2017)

[28] T. Iwasaki, Y. Miyamoto, T. Taniguchi, P. Siyushev, M. H. Metsch, F. Jelezko and M. Hatano, *Tin-vacancy quantum emitters in diamond*, Phys. Rev. Lett. **119**, 253601 (2017)

[29] D. Gatto Monticone, P. Traina, E. Moreva, J. Forneris, P. Olivero, I. P. Degiovanni, F. Taccetti, L. Giuntini, G. Brida, G. Amato and M. Genovese, *Native NIR-emitting single colour centres in CVD diamond*, New J. Phys. **16**, 053005 (2014)

[30] A. Magyar, W. Hu, T. Shanley, M. E. Flatté, E. Hu and I. Aharonovich, *Synthesis of luminescent europium defects in diamond*, Nat. Comm. **5**, 3523 (2014)

[31] J. Forneris *et al., Creation and characterization of He-related color centers in diamond*, J. of Lumin. **179**, 59 (2016)

[32] G. Prestopino *et al.*, *Photo-physical properties of He-related color centers in diamond*, Appl. Phys. Lett. **111**, 111105 (2017)

[33] S. Pezzagna, D. Rogalla, D. Wildanger, J. Meijer and A. Zaitsev, *Creation and nature of optical centres in diamond for single-photon emission – overview and critical remarks*, New J. Phys **13**, 035024 (2011)

[34] I. Aharonovich, S. Casteletto, D. A. Simpson, C.-H. Su, A. D. Greentree and S. Prawer, *Diamond-based single-photon emitters*, Reports on Prog. Phys. **74**, 076501 (2011)

[35] S. Pezzagna et al., *Nanoscale engineering and optical addressing of single spins in diamond*, Small **6**, 2117 (2010).

[36] P. Spinicelli et al., *Engineered arrays of nitrogen-vacancy color centers in diamond based on implantation of CN- molecules through nanoapertures*, New J. Phys. **13**, 025014 (2011).

[37] D. M. Toyli, C. D. Weiss, G. D. Fuchs, T. Schenkel and D. Awschalom, *Chip-scale nanofabrication of single spins and spin arrays in diamond*, Nano Lett. **10**, 3168 (2011)

[38] W. Schnitzler, N. M. Linke, R. Fickler, J. Meijer, F. Schmidt-Kaler and K. Singer, *Deterministic ultracold ion source targeting the Heisenberg limit*, Phys. Rev. Lett. **102**, 070501 (2009)

[39] P. Räcke, D. Spemann, J. W. Gerlach, B. Rauschenbach and J. Meijer, *Detection of small bunches of ions using image charges*, Scientific Reports **??,** ???? (2018)

[40] K. Ohno, F. J. Heremans, L. C. Bassett, B. A. Myers, D. M. Toyli, A. C. B. Jayich, C. J. Palmstrom and D. D. Awschalom, *Engineering shallow spins in diamond with nitrogen delta-doping*, Appl. Phys. Lett. **101**, 082413 (2012)

[41] A. Tallaire et al., *Temperature dependent creation of nitrogen-vacancy centres in single crystal CVD diamond layers*, Diam. Relat. Mater. **51**, 55 (2015).
[42] H. Kato, T. Makino, S. Yamasaki and H. Okushi, *n-type diamond growth by phosphorous doping on (001)-oriented surface*, J. Phys. D: Appl. Phys. **40**, 6189 (2007)
[43] M.-A. Pinault-Thaury, B. Berini, I. Stenger, E. Chikoidze, A. Lusson, F. Jomard, J. Chevallier and J. Barjon, *High fraction of substitutional phosphorous in a (100) diamond epilayer with low surface roughness*, Appl. Phys. Lett. **100**, 192109 (2012)
[44] R. Middleton, *A negative ion cookbook*, (1990).
[45] C. Uzan-Saguy, C. Cytermann, R. Brener, V. Richter, M. Shaanan and R. Kalish, *Damage threshold for ion-beam induced graphitization of diamond*, Appl. Phys. Lett. **67**, 1194 (1995)
[46] J. S. Williams and R. G. Elliman, *Ion beams for material analysis*, Australia: Academic Press (1989)
[47] G. Hobler, *Critical angles and low-energy limits to ion channeling in silicon*, Radiat. Eff. Defects Solids **139**, 21 (1996)
[48] T. E. Derry, R. W. Fearick and J. P. F. Sellschop, *Ion channeling in natural diamond. II. Critical angles*, Phys. Rev. B **26**, 17 (1982)
[49] J. Barjon, F. Jomard and S. Morata, *Arsenic-bound excitons in diamond*, Phys. Rev. B **89**, 045201 (2014)
[50] O. Lehtinen, B. Maydenov, P. Börner, K. Malentjevic, C. Müller, L. P. McGuinness, S. Pezzagna, J. Meijer, U. Kaiser and F. Jelezko, *Molecular dynamics simulations of shallow nitrogen and silicon implantation into diamond*, Phys. Rev. B **93**, 035202 (2016)
[51] M. Posselt, *Crystal-trim and its application to investigations on channeling effects during ion implantation*, Radiat. Eff. Defects Solids **130**, 87 (1994)
[52] R. Schirhagl, N. Raatz, J. Meijer, M. Markham, S. S. A. Gerstl and C. L. Degen, *Nanometer-scale isotope analysis of bulk diamond by atom probe tomography*, Diam. Relat. Mater. **60**, 60 (2015)
[53] M. P. Allen and D. J. Tildesley, *Computer simulation of liquids*, Oxford University Press, Oxford, England (1989)
[54] D. W. Brenner, *Empirical potential for hydrocarbons for use in simulating the chemical vapour deposition of diamond films*, Phys. Rev. B **42**, 9458 (1990)
[55] K. Albe, K. Nordlund and R. S. Averback, *Modeling metal-semiconductor interaction: analytical bond-order potential for platinum-carbon*, Phys. Rev. B **65**, 195124 (2002)
[56] K. Nordlund, N. Runeberg and D. Sundholm, *Repulsive interatomic potentials calculated using Hartree-Fock and density functional theory*, Nucl. Instr. Meth. Phys. Res. B **132**, 45 (1997)
[57] C. A. McLellan, B. A. Myers, S. Kraemer, K. Ohno, D. D. Awschalom and A. C. Bleszynski Jayich, *Patterned formation of highly coherent nitrogen-vacancy centers using a focused electron irradiation technique*, Nano Lett. **16**, 2450 (2016)
[58] J. Ziegler, *The stopping range of ions in matter*, SRIM-2008, online at http://srim.org (2008)
[59] T. Yamamoto, T. Umeda, K. Watanabe, S. Onoda, M. L. Markham, D. J. Twitchen, B. Naydenov, L. P. McGuinness, T. Teraji, S. Koizumi, F. Dolde, H. Fedder, J. Honert, J. Wrachtrup, T. Ohshima, F. Jelezko and J. Isoya, *Extending spin coherence times of diamond qubits by high-temperature annealing*, Phys. Rev. B **88**, 075206 (2013)
[60] S. Pezzagna, B. Naydenov, F. Jelezko, J. Wrachtrup and J. Meijer, *Creation efficiency of nitrogen-vacancy centres in diamond*, New J. Phys. **12**, 065017 (2010).
[61] D. Gatto Monticone, F. Quercioli, R. Mercatelli, S. soria, S. Borini, T. Poli, M. Vannoni, E. Vittone and P. Olivero, *Systematic study of defect-related quenching of NV luminescence in diamond with time-correlated single-phohon counting spectroscopy*, Phys. Rev. B **88**, 155201 (2013).
[62] J. E. Field, *The properties of natural and synthetic diamond*, Academic Press, London, (1992)
[63] J. W. Steeds, T. J. Davies, S. J. Charles, J. M. Hayes and J. E. Butler, *3H luminescence in electron-irradiated diamond samples and its relationship to self-interstitials*, Diam. Relat. Mater. **8**, 1847 (1999)
[64] A. T. Collins, P. J. Woad, G. S. Woods and H. Kanda, *Localised vibrational modes in diamonds grown from mixed carbon isotopes*, Diam. Relat. Mater. **2**, 136 (1993)

[65] A. Lohrmann, S. Pezzagna, I. dobrinets, P. Spinicelli, V. Jacques, J.-F. Roch, J. Meijer and A. M. Zaitsev, *Diamond based light-emitting diode for visible single-photon emission at room temperature*, Appl. Phys. Lett. **99**, 251106 (2011)

[66] N. Mizuochi, *Electrically driven single-photon source at room temperature in diamond*, Nat. Photon. **6**, 299 (2012)

[67] B. Naydenov, R. Kolesov, A. Batalov, J. Meijer, S. Pezzagna, D. Rogalla, F. Jelezko and J. Wrachtrup, *Engineering single photon emitters by ion implantation in diamond*, Appl. Phys. Lett. **95**, 181109 (2009)

[68] I. A. Dobrinets, V. G. Vins, A. M. Zaitsev, HPHT-treated diamonds, Springer (2013)

[69] S. Pezzagna and J. Meijer, *High-resolution implantation from keV to MeV*, chapter in Ion Implantation, InTech, Editor Mark Goorsky, ISBN 978-953-51-0634-0 (2012)

[70] B. Naydenov et al., *Enhanced generation of single optically active spins in diamond by ion implantation*, Appl. Phys. Lett. **96**, 163108 (2010)

[71] F. Fávaro de Oliveira, D. Antonov, Y. Wang, P. Neumann, S. A. Momenzadeh, T. Häußermann, A. Pasquarelli, A. Denisenko and J. Wrachtrup, *Tailoring spin defects in diamond by lattice charging*, Nat. Comm. **8**, 15409 (2016)

[72] D. Antonov *et al.*, *Statistical investigations on nitrogen-vacancy center creation*, Appl. Phys. Lett. **104**, 012105 (2014)

[73] M. Lesik, N. Raatz, A. Tallaire, P. Spinicelli, R. John, J. Achard, A. Gicquel, V. Jacques, J.-F. Roch, J. Meijer and S. Pezzagna, *Production of bulk NV centre arrays by shallow implantation and diamond CVD overgrowth*, Phys. Stat. Sol. A **213**, 2594 (2016)

[74] L. Allers, A. T. Collins and J. Hiscock, *The annealing of interstitial-related optical centres in type II natural and CVD diamond*, Diam. Relat. Mater. **7**, 228 (1998)

[75] R. Jones, J. P. Goss, H. Pinto and D. W. Palmer, *Diffusion of nitrogen in diamond and the formation of A-centres*, Diam. Relat. Mater. **53**, 35 (2015)

[76] H. Kato, H. Watanabe, S. Yamakasi and H. Okushi, *N-type doping on (001)-oriented diamond*, Diam. Relat. Mater. **15**, 548 (2006)

[77] R. U. A. Khan, B. L. Cann, P. M. Martineau, J. Samartseva, J. J. P. Freeth, S. J. Sibley, C. B. Hartland, M. E. Newton, H. K. Dhillon and D. J. Twitchen, *Colour-causing defects and their related optoelectronic transitions in single crystal CVD diamond*, J. Phys.: Condens. Mater. **25**, 275801 (2013)

[78] E. Fritsch, T. Hainschwang, L. Massi and B. Rondeau, *Hydrogen-related optical centers in natural diamond : an update*, New Diam. And frontier carbon technol. **17**, 63 (2007)

[79] A. Stacey, T. J. Karle, L. P. McGuinness, B. C. Gibson, K. Ganesan, S. Tomljenovic-Hanic, A. D. Greentree, A. Hoffman, R. G. Beausoleil and S. Prawer, *Depletion of nitrogen-vacancy color centers in diamond via hydrogen passivation*, Appl. Phys. Lett. **100**, 071902 (2012)

[80] I. Z. Machi, J. E. Butler, S. H. Connell, B. P. Doyle, R. D. Maclear, J. P. F. Sellschop, E. Sideras-Haddad and D. B. Rebuli, *Diffusion characteristics of hydrogen in diamond*, Diam. Relat. Mater. **8**, 1611 (1999)

[81] J. Barjon et al., *Hydrogen-induced passivation of boron acceptors in monocrystalline and polycrystalline diamond*, Phys. Chem. Chem. Phys. **13**, 11511 (2011)

[81b] J. C. Arnault, S. Saada, C. Mer-Calfati, F. Jomard, N. Habka, J. Barjon and J. Chevallier, *Enhanced deuterium diffusion in boron doped monocrystalline diamond films using bias-assisted MPCVD*, Phys. Lett. A **374**, 3254 (2010)

[82] T. Staudacher, F. Ziem, L. Haussler, R. Stohr, S. Steinert, F. Reinhard, J. Scharpf, A. Denisenko and J. Wrachtrup, *Enhancing the spin properties of shallow implanted nitrogen vacancy centers in diamond by epitaxial overgrowth*, Appl. Phys. Lett. **101**, 212401 (2012)

[83] S. W. Hell and J. Wichmann, *Breaking the diffraction resolution limit by stimulated emission: stimulated-emission-depletion fluorescence microscopy*, Opt. Lett. **19**, 780 (1994).

[84] A. Collins, *The Fermi level in diamond*, J. Phys. Cond. Mater. **14**, 3743 (2002)

[85] M. J. Rust, M. Bates and X. Zhuang, *Sub-diffraction-limit imaging by stochastic optical reconstruction microscopy (STORM)*, Nat. Methods **3**, 793 (2006)

[86] E. Betzig, G. H. Patterson, R. Sougrat, O. Wolf Lindwasser, S. Olenych, J. S. Bonifacino, M. W. Davidson, J. Lippincott-Schwartz and H. F. Hess, *Imaging intracellular fluorescent proteins at nanometer resolution*, Science **313**, 1642 (2006)

[87] K. Groot-Berning, N. Raatz, I. Dobrinets, M. Lesik, P. Spinicelli, A. Tallaire, J. Achard, V. Jacques, J.-F. Roch, A. M. Zaitsev, J. Meijer and S. Pezzagna, *Passive charge state control of nitrogen-vacancy centres in diamond using phosphorous and boron doping*, Phys. Stat. Sol. A **211**, 2268 (2014)

[88] Y. Doi et al., *Pure negatively charge state of the NV center in n-type diamond*, Phys. Rev. B **93**, 081203(R) (2016)

[89] L. Rondin *et al.*, *Surface-induced charge state conversion of nitrogen-vacancy defects in nanodiamonds*, Phys. Rev. B **82**, 115449 (2010)

[90] M. V. Hauf *et al.*, *Chemical control of the charge state of nitrogen-vacancy centers in diamond*, Phys. Rev. B **83**, 081304(R) (2011)

[91] S. Y. Cui and E. H. Hu, *Increased negatively charged nitrogen-vacancy centers in fluorinated diamond*, Appl. Phys. Lett. **103**, 051603 (2013)

[92] C. Osterkamp, J. Scharpf, S. Pezzagna, J. Meijer, T. Diement, R. J. Behm, B. Naydenov and F. Jelezko, *Increasing the creation yield of shallow single defects in diamond by surface plasma treatment*, Appl. Phys. Lett. **103**, 193118 (2013)

[93] X.-D. Chen, C.-L. Zou, F.-W. Sun and G-C Guo, *Optical manipulation oft he charge state of nitrogen-vacancy center in diamond*, Appl. Phys. Lett. **103**, 013112 (2013)

[94] M. V. Hauf *et al.*, *Addressing single nitrogen-vacancy centers in diamond with transparent in-plane gate structures*, Nano Lett. **14**, 2359 (2014)

[95] M. Shimizu, T. Makino, T. Iwasaki, K. Tahara, H. Kato, N. Mizuochi, S. Yamasaki and M. Hatano, *Charge-state control of ensemble of nitrogen vacancy centers by n-i-n diamond junctions*, Appl. Phys. Exp. **11**, 033004 (2018)

[96] N. Aslam, G. Waldherr, P. Neumann, F. Jelezko and J. Wrachtrup, *Photo-induced ionizazion dynamics oft he nitrogen vacancy defect in diamond investigated by single-shot charge state detection*, New J. Phys. **15**, 013064 (2013)

[97] B. Ofori-Okai, S. Pezzagna, K. Chang, M. Loretz, R. Schirhagl, Y. Tao, B. A. Moores, K. Groot-Berning, J. Meijer and C. Degen, *Spin properties of very shallow nitrogen vacancy defects in diamond*, Phys. Rev. B **86**, 081406(R) (2012)

[98] G. Balasubramanian *et al.*, *Ultralong spin coherence time in isotopically engineered diamond*, Nat. Mater. **8**, 383 (2009)

[99] A. Dréau, J.-R. Maze, M. Lesik, J.-F. Roch and V. Jacques, *High-resolution spectroscopy of single NV defects coupled with nearby 13C nuclear spins in diamond*, Phys. Rev. B **85**, 134107 (2012)

[100] L. Thi Mai Hoa, T. Ouisse, D. Chaussende, M. Naamoun, A. Tallaire and J. Achard, *Birefringence microscopy of unit dislocations in diamond*, Cryst. Growth Des. **14**, 5761 (2014)

[101] E. Rittweger, K. Y. Han, S. E. Irvine, C. Eggeling and S. W. Hell, *STED microscopy reveals crystal colour centres with nanometric resolution*, Nat. Photon. **3**, 144 (2009)

[102] A. A. Gippius, *Impurity-defect reactions in ion-implanted diamond*, Materials Sci. Forum **83**, 1219 (1992).

[103] H. Hofsäss, M. Dalmer, M. Restle and C. Ronning, *Substitutional phosphorous doping of diamond by ion implantation*, J. Appl. Phys. **81**, 2566 (1997)

[103b] J. Barjon, new cathodo measurements

[104] J. P. Goss, P. R. Briddon, M. J. Rayson, S. J. Sque and R. Jones, *Vacancy-impurity complexes and limitations for implantation doping of diamond*, Phys. Rev. B **72**, 035214 (2005)